4-11-2013 12:00 AM

Numerical Modelling of Species Exchange in a 3D Porous Medium: Modelling Exchange Within the Human Lung

Chelsea E. Johnson
The University of Western Ontario

Supervisor
Anthony G. Straatman
The University of Western Ontario

Graduate Program in Mechanical and Materials Engineering
A thesis submitted in partial fulfillment of the requirements for the degree in Master of Engineering Science

Numerical Modelling of Species Exchange in a 3D Porous Medium: Modelling Exchange Within the Human Lung

(Thesis format: Monograph)

by

Chelsea E. Johnson

Graduate Program in Engineering Science

Department of Mechanical and Materials Engineering

A thesis submitted in partial fulfillment
of the requirements for the degree of
Master of Engineering Science

The School of Graduate and Postdoctoral Studies
The University of Western Ontario
London, Ontario, Canada

ABSTRACT

The volume-averaged oxygen transport equation is closed using a volume-averaged form of Fick's law of diffusion between the air and tissue to simulate species exchange within the lungs' alveoli using a computational fluid dynamics (CFD) 3D conjugate domain model. Pore level simulations of a terminal alveolated duct are used to determine that the transport of inhaled oxygen from the cluster inlet to the alveolar walls is diffusion dominated. The resistance to oxygen diffusion into the tissue is found to be a function of the tidal volume and tissue transport properties, with a maximum respiration frequency at which the full amount of oxygen available can be exchanged per breath dependent on the tidal volume. The simulated exhaled oxygen and carbon dioxide compositions match experimental values for regular resting respiration. Therefore, this model provides a viable new approach to modelling species exchange within the alveoli.

Keywords: *CFD, porous media, volume averaging, species exchange, human lung, terminal alveolated cluster*

ACKNOWLEDGEMENTS

The past two years of work completed for this thesis would not have been possible without the following people:

Dr. Anthony Straatman

Dr. Christopher DeGroot

Christian Fischer

Their assistance in understanding and completing this work was greatly appreciated. I would also like to acknowledge my family and remaining colleagues for their support.

I would like to thank the financial support of NSERC, OGS and the family of Richard Dillon who sponsored one third of my OGS award in his name. Without these contributions, completing this thesis would not have been possible.

- Chelsea E. Johnson

TABLE OF CONTENTS

LIST OF TABLES

LIST OF FIGURES

NOMENCLATURE

ROMAN LETTERS

A	area, m^2
A_{fs}	interface between the fluid and solid constituents, m^2
a_{sf}	interfacial area per unit volume, m^{-1}
C	critical SAVR value
c_A	molar concentration per volume of species A, mol/kg
C_E	tensor used in momentum closure
D	diffusion coefficient, m^2/s
D_f	diffusion coefficient of species A in the fluid constituent, m^2/s
D_s	diffusion coefficient of species A in the solid constituent, m^2/s
D_H	hydraulic diameter, m
D_ϕ	diffusion coefficient of species ϕ, m^2/s
$\mathbf{f}$	body force per unit mass, m/s^2
f	frequency of respiration, Hz
i	index of integration point
J	mass flux of species A, mol·m/s
K	scalar permeability of the porous medium, m^2
k	average exchange coefficient, m/s
K_{eq}	absorption coefficient, m
L	macroscopic length scale, m
l	pore-level length scale, m
$\dot{m}_i$	mass flux of constituent i, kg/s
$\widehat{M}$	molar mass, kg/kmol
N_A	maximum amount of oxygen exchanged per breath, mol
$\dot{N}_A$	maximum amount of oxygen exchanged per second, mol/s
$\mathbf{n}_{fs}$	unit-normal vector directed from the fluid to solid constituent
n	constant relating SAVR to the critical value
p	pressure, Pa
p_i	partial pressure of i, Pa

P_{tot} total pressure of the mixture, N/m^2

Pe Peclet number

R resistance to diffusion, s

Re Reynolds number

Sc Schmidt number

T temperature, °C or K

t time, s

t_D time scale of diffusion, s

t_R time scale of respiration, s

$\mathbf{u}$ fluid velocity vector, m/s

u x component of velocity, m/s

v y component of velocity, m/s

V volume contained within averaging volume, m^3

V_i volume of constituent i contained within V, m^3

V_f volume of the fluid contained within V, m^3

V_s volume of the solid contained within V, m^3

V_p volume of control volume P, m^3

V_T tidal volume of the terminal alveolated cluster, m^3

$\dot{V}_{gas}$ rate at which gas is diffused in a simplified form of Fick's law

w z component of velocity, m/s

y_i mole fraction of i

GREEK LETTERS

Δ change in a property

∇ gradient

α_A solubility of species A in the tissue, kg/m^3

μ dynamic viscosity of the fluid, kg/m·s

φ generic transport variable

ρ density, kg/m^3

ρ_f density of the fluid, kg/m^3

ε porosity

ω angular frequency of respiration, s^{-1}

SUBSCRIPTS

f fluid

s solid

i quantity evaluated at integration point

SYMBOLS

$\langle\varphi\rangle$ extrinsic average of quantity φ

$\langle\varphi\rangle^f$ intrinsic average of quantity φ with respect to the fluid phase

$\langle\varphi\rangle^s$ intrinsic average of quantity φ with respect to the solid phase

$\tilde{\varphi}$ spatial deviation of a quantity φ

ABBREVIATIONS

SAVR Surface area to volume ratio available for diffusion

CHAPTER 1

INTRODUCTION

1.1 PHYSIOLOGICAL BACKGROUND

All cells within the human body require oxygen to survive; for this reason the respiratory system is vital to our existence. The respiratory system coordinates the intake of oxygen from the air and the release of carbon dioxide back into the air. Oxygenated blood is carried from the lungs, by the circulatory system, throughout the body before deoxygenated blood is returned to the lungs to be refreshed. This complex oxygen transport system evolved once passive transport was no longer sufficient to supply oxygen to increasingly larger organisms [1]. Figure 1.1 shows the basic anatomy of the human lung. This terminology will be used throughout the remainder of this work.

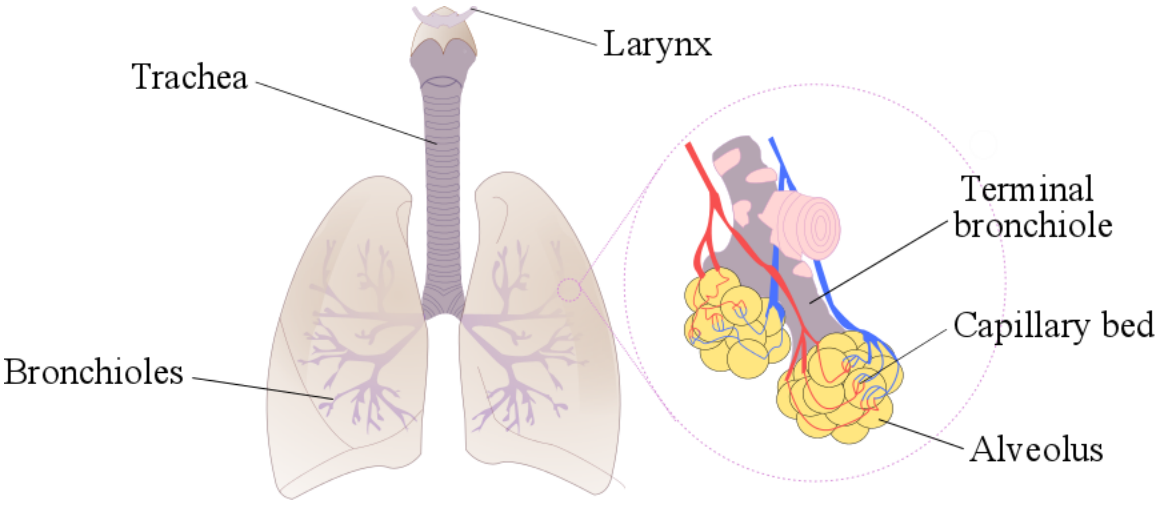

Figure 1.1. *Human respiratory system, two terminal alveolated clusters are included.*

During inhalation, air passes through approximately twenty-three vessel bifurcations between the trachea and the alveoli [1-5]. The largest vessels within the lungs are the first three generations of bronchi, with diameters greater than 0.5 cm. These connect to thirteen generations of bronchioles. These bronchioles have an approximate diameter of 0.05 cm with a length of 0.1 cm, and eventually feed the alveoli [2].

Gas exchange between the air and blood occurs within each alveolus. An alveolus (plural: alveoli) is the small sac of air that partially inflates upon inhalation and partially deflates upon exhalation. The anatomy of an alveolus is specialized to maximize the surface area available for exchange between the blood and alveolar air. The volume of air inhaled with each resting breath is approximately 0.5 litres for an adult male [4]. This value is known as the tidal volume and should not be confused with the functional residual capacity, which describes the volume of air remaining within the lungs once the tidal volume has been exhaled. The functional residual capacity prevents the lungs from collapsing and has an approximate volume of 3.2 litres for an adult male [4]. With this air retention, a pulmonary volume change of approximately 15% is associated with tidal breathing.

The thin cell layer, which constitutes the alveolar wall, is known as the blood-gas barrier. This layer is less than one micron thick in places [1]. The transport of oxygen (O_2) and carbon dioxide (CO_2) across this barrier is solely the product of passive diffusion driven by the partial pressure difference of the individual gases on either side [1-5,8]. With roughly 300 million alveoli in each lung, the surface area available for exchange is approximately 70 m^2 [3]. In reality multiple capillaries, known as a capillary bed, surround each alveolus, although only a couple of capillaries are shown in Figure 1.1. An alveolus is the final destination of air within the lung, both entering and exiting through the same opening. During exhalation, air retraces the same path taken during inhalation before leaving the body.

Due to the delicate nature of the blood-gas barrier, the inhaled air must be altered prior to reaching the alveoli, its final destination. The specialized function of the nasal cavity contributes much of the moistening, filtering and warming of the air, although the same function can occur further into the respiratory system if necessary when air is inhaled through the mouth [3]. Once the air reaches the larynx it has been fully heated to body temperature [2]. Prior to reaching the alveolar walls, the water vapour content of the inhaled air has reached its saturation point, ensuring the lungs' internal surfaces remain moist at all times [5]. The need for a moist exchange surface is the reason land animals

have developed internal respiratory systems while fish are able to breath with an external method (gills).

A human lung contains between 70 ml and 140 ml of blood spread across the 70 m^2 surface area [3]. This blood spends approximately one second in the capillary bed surrounding the alveoli before being replaced [6]. As a result, the oxygen and carbon dioxide exchange rates must be relatively fast to reflect the continual output of the heart [6]. By comparison, the volume of air within the lungs at any given point in time is much greater than the volume of blood.

The compositions of both inhaled air and exhaled air are given in terms of partial pressure in Table 1.1. Inhaled air and atmospheric air are the same; therefore the composition of the inhaled air given in Table 1.1 is equivalent to atmospheric air.

Table 1.1. *Composition of the gaseous components in air [4] along with the molar mass of the relevant gases*

	Inhaled Air	**Exhaled Air**	**Molar Mass**
Nitrogen	78%	78%	28.0134 kg/kmol
Oxygen	21%	17%	31.9988 kg/kmol
Carbon dioxide	0.04%	4%	44.01 kg/kmol
Inert gas	0.96%	1%	NA
Water vapour	Variable	Saturated	NA

Negative pressure breathing is caused by muscle contractions increasing the lungs' volume and expanding the alveoli. This expansion causes the alveolar pressure to decrease below atmospheric pressure, allowing air to be drawn into the lungs during inhalation [2]. Assuming the pressure at the entrance to the lung is atmospheric, the partial pressures of both O_2 and CO_2 can be obtained using the compositions given in Table 1.1. The partial pressures of oxygen and carbon dioxide can be calculated using

$$p_i = y_i \cdot P_{tot} \tag{1.1}$$

where p_i is the partial pressure of i, y_i is the composition or mole fraction of i and P_{tot} is the total pressure of the mixture. Therefore the partial pressure of oxygen during inhalation is approximately 21.0 kPa and 14.7 kPa during exhalation [9]. The partial pressure of carbon dioxide during inhalation is 0.04 kPa and 4.1 kPa during exhalation.

The partial pressures of both oxygen and carbon dioxide in the blood have been experimentally determined. Table 1.2 gives the partial pressure values for various gases in the blood and the alveolar air as given by Waugh and Grant [4].

Table 1.2. *Experimental partial pressure values for various gases within the lungs [4].*

	Alveolar air		**Deoxygenated blood**		**Oxygenated blood**	
	kPa	mmHg	kPa	mmHg	kPa	mmHg
Oxygen	13.3	100	5.3	40	13.3	100
Carbon dioxide	5.3	40	5.8	44	5.3	40
Nitrogen and other inert gases	76.4	573	76.4	573	76.4	573
Water vapour	6.3	47				
	101.3	**760**				

1.2 IMPORTANCE OF MODELLING

The importance of the lungs' function can not be denied, however studying the lungs can be difficult due to their complex geometry and function. Although it is possible to measure airflow and composition changes in vivo [7,10-11], these studies are generally limited to macroscopic measurements. To study species exchange and airflow within the lungs, models are developed [13-17,19-20,22-27]. Modelling a fully functioning lung has not been possible in the past due to its complex geometry, however with advancements in computing technology, this is now reasonable [17,23-24]. Models can be used for flow simulations [13-17,24], for particle dispersion [16,19] and for species exchange [23]. Parameters within the simulations can be altered to reflect various forms

of lung damage without negatively affecting a test subject. Therefore, it is important for models to accurately predict experimental values.

Many different approaches are being used to model the respiratory system [13-17,19-22,25-27]. Various approaches will be discussed further in Chapter 2.

1.3 OBJECTIVES

Due to the porous nature of the alveoli's structure, a three-dimensional finite-volume porous media computational fluid dynamics (CFD) model can be used to represent the lung. The model developed by Betchen et al [8] can be adapted to mimic the properties of a human lung and used to model the oxygen and carbon dioxide transport with the lungs' alveoli. This thesis will develop a framework for modelling oxygen and carbon dioxide exchange within a porous media CFD three-dimensional code. With this framework in place, the proposed model can be adapted for use in other studies including the absorption of medications or toxins.

1.4 GENERAL APPROACH TO THE PROBLEM

Modelling the entire lung was not necessary due to the complexity of the lungs' geometry, therefore this work focused on modelling a small tissue sample representing a section of terminal alveoli. The sample size of the tissue was arbitrarily set to 6.0 cm × 4.0 cm × 2.0 cm as these dimensions correspond with a reasonable section of terminal alveoli in the human lung. The finite volume method was used to divide the porous domain into small volumes over which the necessary governing equations were solved to complete the simulation. Due to the nature of porous media modelling, calculating the results for each individual pore would be too computationally expensive. Therefore, the equations are first volume averaged allowing the average value of the required variable be determined.

Modelling a full breathing cycle requires the same inlet and outlet as well as an expanding porous structure to accommodate mass conservation. As an expanding porous structure was beyond the scope of this work, a separate inlet and outlet were used in conjunction with a rigid porous structure. To represent natural breathing cycles, sinusoidal waveforms were modelled over the course of the simulation. Air was moved through the porous alveolar sample to simulate breathing. Since species exchange occurs solely within the alveoli [9], without accounting for a changing surface area, simulating the air reaching the terminal alveoli was made possible by solving for species exchange over a small period of time when the velocity of the air passing through the porous medium was near zero.

1.5 SCOPE OF THE PROJECT

The purpose of this study was to develop a framework for modelling oxygen and carbon dioxide exchange by introducing a species transport equation into an existing 3D conjugate code. In order to implement oxygen exchange between the fluid and solid constituents of the porous medium the species transport equation must be volume averaged to account for the effects of the pore geometry within the porous structure. Pore level simulations were completed to properly understand oxygen transport within the terminal alveoli. With this information, it was possible to integrate the pore level simulation results with the volume-averaged species transport equation and simulate the changes in air composition as it passed through the simulated lung sample. Once oxygen exchange was properly embodied in the existing 3D conjugate code, adding carbon dioxide exchange made this model unique in its approach to simulating species exchange within the lung.

1.6 OUTLINE OF THESIS

The remaining chapters in this thesis outline how the framework for modelling oxygen and carbon dioxide exchange within a 3D porous media CFD code was developed and implemented. The chapters are as follows:

- **Chapter 2:**
  The literature review comparing the approaches of previous lung models, and the void the present model will fill once complete. This chapter also includes current models closely pertaining to this work.

- **Chapter 3:**
  The development of the mathematical model used to simulate oxygen exchange between the air and the tissue, including the volume averaging and discretization of the mass and momentum equations.

- **Chapter 4:**
  Pore level simulations completed to understand how the resistance to diffusion is affected by the properties of the alveolar air, and to determine the conditions at which each alveolus operates.

- **Chapter 5:**
  This chapter covers the closure of the volume-averaged oxygen transport equation and the finalization of the average exchange coefficient modelling method. The effects of the tissue parameters on the diffusion are examined here with simulations shown proving the viability of the present model.

- **Chapter 6:**
  A summary of the present work is supplemented by the contributions made, along with the recommendations for future work.

CHAPTER 2

LITERATURE REVIEW

2.1 PHYSIOLOGICAL MODELS

For many years people have been using engineering techniques to model physiological phenomena [13-17,19-27]. This makes separating purely physiological models difficult, therefore discussed here are preliminary models superseding the engineering models discussed in Section 2.2.

When focusing on oxygen diffusion within the lungs, a unique problem is encountered. Current physiological models examine pulmonary oxygen transport by focusing on the microscopic scale. Species transport equations are based on blood flow through single capillaries using Fick's law of diffusion as the basis for these models [3]. The difference in the partial pressure of oxygen between the alveoli and the blood is introduced as the gradient driving diffusion [9]. The rate of gas transfer or diffusion is

$$\dot{V}_{gas} \propto \frac{A}{L} \cdot D \cdot (p_1 - p_2) \tag{2.1}$$

where A is the surface area available for diffusion, L is the thickness of the tissue, p_1 and p_2 are the partial pressures on either side of the tissue, $\dot{V}_{gas}$ is the rate at which the gas diffused, and the diffusivity constant is

$$D \propto \frac{1}{\widehat{M}} \tag{2.2}$$

where $\widehat{M}$ is the molar mass of the gas. The amount of gas diffused is directly proportional to the area available for diffusion and inversely proportional to the thickness of the tissue [9]. The diffusivity constant of the gas within the tissue is proportional to the gas' solubility yet inversely proportional to its molecular weight [9].

To compensate for the lack of solely physiological modelling progress, there is plenty of research into lung functionality using experimental data [7,10-11]. Spirometers are used to measure air velocities during respiration, while other equipment can measure the composition of the air during exhalation [7]. Studying exchange within the lungs has been accomplished with carbon monoxide studies [10]. Red blood cells have a greater affinity for carbon monoxide than oxygen; therefore studying the exchange of this gas is easier than studying oxygen [10]. These studies [7,10-11,22] can be used to help calibrate and validate engineering models.

To study lung geometry animal studies are often used, as mammalian lung anatomies are very similar. Scanning Electron Microscope images of alveoli (both human and animal), as seen in Figure 2.1, are the images commonly associated with lungs.

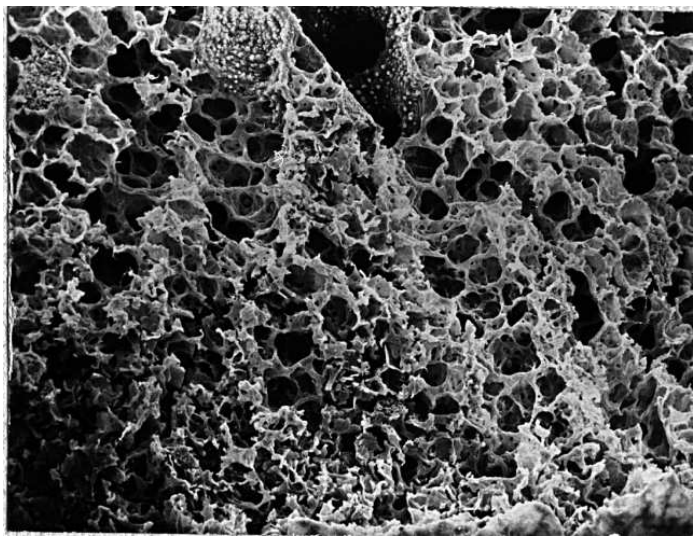

Figure 2.1. *Scanning Electron Microscope image of a mouse lung showing a terminal bronchiole, with surrounding alveoli. Note the alveoli are closely packed against each other and share walls (septa). Images of a mouse lung obtained from the Lawrence Berkeley national Laboratory Lung Lab Tour, http://imglib.lbl.gov/TmgLib/COLLECTIONS/LUNGSTRUCTURE/.tour/page1.htm*

These images and the accompanying histological data can only be recovered once the animal has been sacrificed and the lungs removed [11]. Studying species exchange on the alveolar level is not possible through current experimental means; this is where more complex engineered physiological models are needed.

2.2 ENGINEERING MODELS

To properly model the total oxygen and carbon dioxide transfer within the lungs, they must be examined on a macroscopic scale. Therefore, the complex porous structure of the alveoli must be modelled in conjunction with the air movement through the lungs [12,22,27].

2.2.1 Upper Airway Models

Most engineering studies of airflow within the lungs have focused primarily on the upper airways with the use of conventional computational fluid dynamics (CFD) techniques [13]. The airway tree has been modelled as a one-dimensional bifurcating system with the number of bifurcations dependent on minimizing the resistance to oxygen transport through the alveolar wall [14] and lead to the optimal bifurcation number.

Modelling the upper airway often includes the trachea and mouth [15-16]. MRI data has been used to reconstruct the thorax to model vapour transport within the upper airway [15] as this region saturates the air prior to reaching the alveoli. Other models use scanned molds of the thorax, prior to a simplified bifurcation or two within the lung itself [16]. These simulations reveal that the turbulent flow produced by the geometry of the upper airway proceeds into the lungs themselves [16]. However, by the time air has reached the alveoli, the flow is laminar.

The model proposed by Gemci et al [17] uses CFD techniques to model the first 17 generations of the airway tree. This model predicts a pressure drop of 50 Pa between the opening of the trachea and the alveoli as well as the transition from turbulent airflow in the upper airway to laminar airflow before the second bifurcation [17]. However, approximately 90% of air volume resides within the 17^{th} to 23^{rd} generation of the lung [18], not modelled by Gemci et al [17].

2.2.2 Terminal Airway Models

Engineering models for the lower branches of the airway tree have focused primarily on the parenchyma region of the lung [19-22]. This region is where species exchange

occurs, containing numerous acinar clusters of alveoli. Although these models focus solely on airflow, neglecting species exchange [19-21]. Due to the complex porous structure of the alveoli, the geometry used to model single acinar regions (terminal bronchioles surrounded by clustered alveoli) varies across the studies.

There are two models of interest incorporating different idealized acinar geometries for airflow simulations [19-20]. Harding et al [19] developed a 3D CFD model of a pulmonary acinus with expanding spherical alveoli equally spaced about a rigid, circular duct, refer to Figure 4.1. A total volume change of 15.6% was simulated during inhalation without allowing the 13 simulated alveoli to contact one another. Kumar et al [20] used 19 truncated octahedron shaped alveoli nestled together to better simulate the interaction between the individual alveoli, refer to Figure 4.2. Their acinar model simulated a 25% volume expansion with each breath. Neither Harding et al [19] nor Kumar et al [20] noted any recirculation present within the acinar region. However, when an alveolated duct with through flow was tested, recirculation was noted in each alveolus [20].

Particle Image Velocimetry (PIV) has been used with limited success for modelling terminal acinar clusters [21]. Oakes et al [21] used an expanding geometry similar to the one proposed by Harding et al [19]. Due to the PIV requirement for clear container walls (i.e. the walls of the acinar cluster), a new expanding material with limited testing was used [21]. Oakes et al [21] noted inhaled fluid did not penetrate through to the furthest alveolus. Instead, fresh fluid came less than half way into the cluster before being exhaled [21].

2.2.3 Alveolar Region Models

Tsuda et al [22] recognized the need to model alveoli with a larger, integrated structure unlike the approaches described above. With the use of synchrotron X-ray tomography images of rat lungs, they reconstructed a 3D model of the parenchyma region using the finite element method [22]. Tsuda [22] matched the volume density of tissue in their model to within 2% of their gold standard biological value of 0.196 [11]. Unfortunately, their surface area density remained below their expected value of 904 cm^2/cm^3 [11,22].

The difference between the histological measurement techniques [11] and the modern imaging techniques [22] used for the lung samples resulted in this discrepancy. Their technique to reconstruct the porous geometry of the alveolar region is unique and can be used in future work studying fluid flow and species transportation in this region.

2.2.4 Alveolar Porous Media Models

Porous media CFD models are increasingly being used to model biological components [23-27]. Existing models closely related to the work introduced in this thesis are those used for modelling arteries [23-24] and the human lung [25-27]. Yang et al [23] introduced species transport through porous media tissue layers surrounding arteries. Their use of volume averaged governing equations along with coupled species transport equations in the arterial lumen and the arterial walls were able to replicate transport of low-density lipoprotein (LDL) through these walls [24]. This approach to arterial transport can be applied to other biological settings and other porous media models.

A previous study by Koulich et al [25] used a porous media model to study alveolar gas diffusion. They proposed that a porous domain could represent the terminal alveoli. The diffusive capacity of the lungs was determined by studying the diffusion of carbon monoxide (CO) into the solid constituent [25]. They ignored the need to study airflow within the porous structure and volume-averaged Fick's law of diffusion driven by partial pressure changes. Simulated sinks spaced throughout the solid constituent, or tissue, simulated the presence of red blood cells. By increasing the density of these sinks, they determined the cells in the centre of the domain showed no signs of diffusion, as the CO present at the boundaries was absorbed prior to diffusing through to the centre of the model [25]. Their results showed that the effective diffusion coefficient was much closer to the diffusion value of the tissue than to the diffusion value of the air; consistent with the tissue having a greater effect on the diffusion than the alveolar air.

2.2.5 Macroscopic Lung Models

Two different approaches to applying porous media regions in CFD models have been included in this review. Both models use a porous medium to simulate the lower parts of the lung while using conventional CFD to simulate the upper airways. The first method

uses the bifurcating airway tree approach developed by Nakayama et al [14] and incorporates oxygen and carbon dioxide exchange [26]. This model predicts the existence of exactly 23 levels of bifurcation between the trachea and the terminal alveoli, however large assumptions were made to derive this value. It was assumed species exchange occurs within the entire lung (both the alveoli and the upper airways) [14,26] although this is known to be incorrect [9]. The full bifurcating airway tree model terminated at a porous media wall simulating the blood-gas barrier. Oxygen exchange was simulated again in this region [25]. Although the governing equations in the porous region have been altered to reflect the assumption exchange occurs prior to reaching the alveoli, this model simulates a species exchange which is not included in the alternate approach discussed.

The second approach using porous media to model the lung is proposed by DeGroot [27]. In the lower airways and alveoli, there are far too many paths to use conventional CFD techniques due to current limitations in processor speed and memory. Thus, to simulate flow and exchange in this region of the lung, models are required to consider the airflow in an averaged sense to have a problem of reasonable size [27]. However, these models are in their infancy for physiological applications and require further development to improve their accuracy. DeGroot [27] developed a porous media CFD model using an expanding domain with an unstructured grid, thereby providing a capable new model for various engineering and physiological applications. As described previously, the interior of the lungs resemble a porous media due to the unique configuration of the alveoli to maximize the surface area available for species exchange. Treating the lower regions of the lungs as a porous domain decreases computational time by simplifying the method for modelling airflow and species exchange.

This is the only porous media model in existence with the capability to integrate an upper airway tree feeding into a porous media structure simulating the lower airways and terminal alveoli. The model proposed by DeGroot [27] used CT images to segment the lungs into a limited bifurcating airway tree and porous media structure [27]. The geometry used in this model can be seen in Figure 2.2.

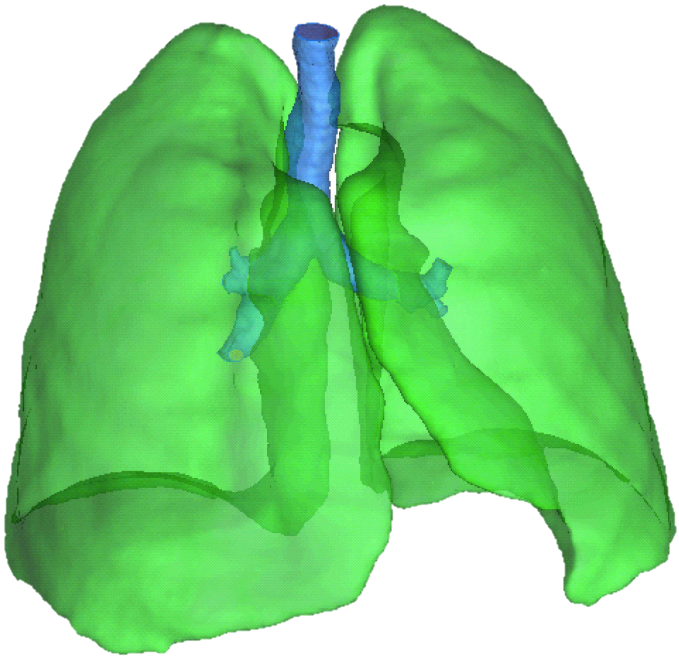

Figure 2.2. *Diagram of the lung model developed by DeGroot [27] showing the bifurcating airway tree (blue) and the porous lung tissue (green). Image taken from DeGroot [27].*

The alterations made to the geometry allowed for proper interface conditions between the airway tree and surrounding porous media to be applied. Sinusoidal respiration was introduced by controlling the motion of the diaphragm at the bottom of the lung [27].

DeGroot [27] assumed the permeability of the lung could be approximated from the permeability of an alveolated duct, the average permeability was given as

$$K/\varepsilon = 1.75\times10^{-9}\ \text{m}^2 \tag{2.3}$$

which was valid for an average diameter of 0.43 mm, the weighted average of the airway diameters between the 17$^{\text{th}}$ and 23$^{\text{rd}}$ generations [18]. Weibel's [18] porosity of $\varepsilon = 0.9$ gave an estimated permeability of $K = 1.58\times10^{-9}$ m^2 [27]. DeGroot [27] assumed the hydraulic diameters of the ducts and the porosity varied sinusoidally with time, resulting in lung permeability given as function of time

$$K = K_0[1 + A_\varepsilon \cos(\omega t)]\left[1 + A_{D_H} \cos(\omega t)\right]^2 \tag{2.4}$$

where K_0 is the permeability at mean inflation, A_{D_H}= 0.025 is the amplitude of the diameter changes and A_ε was set to zero [27].

This model replicated a pressure drop of 50 Pa [17] between the mouth and the terminal alveoli with slightly fewer than one million tetrahedral control volumes [27]. The airway model proposed by Gemci et al [17] discussed earlier used approximately 6.7 million control volumes without achieving grid independence. Therefore the new porous media model by DeGroot [27] is capable of replicating previous results with significantly less control volumes than conventional CFD pulmonary models.

Implementing oxygen and carbon dioxide transport into the model developed by DeGroot [27] would be a first among other engineering and physiological lung models. This model would have potential use in various studies [22,27] (i.e. geometry specific studies, exchange simulations, particle transport, etc.) to study the effects of pathological changes on the absorption of oxygen and other inhaled substances such as medications or toxins. Before species transfer can be included into a model of this complexity, an exchange model needs to be developed for a simplified porous domain. The development of this intermediate model is the purpose of the present work and will be described in detail throughout the upcoming chapters.

CHAPTER 3

MODEL FORMULATION

This chapter will describe the approach used to integrate oxygen transport into a 3D conjugate model. This discussion will cover two domains: fluid and porous. Special considerations required along the interfaces between the domains are not included here, as these were preexisting in the model [8]. Alterations required for the oxygen transport equation calculations within the porous domain will be discussed in detail along with a brief description of how the governing equations were discretized. The volume averaging of the oxygen transport equations in both the fluid and solid constituent will also be included.

3.1 APPROACH

3.1.1 Respiration Cycle

Transient simulations, like respiration modelled in this work, require a sufficient number of washout cycles before the effects of the initial conditions have been eliminated. Once the effects have disappeared, the results are considered to be time-periodic with each simulated cycle modelling the same values for every corresponding time frame. Therefore a sufficient number of breath cycles need to be simulated to ensure the initial effects have washed out before results are recorded.

By the time inhaled air reaches the region of study for this model, it has passed through the entire airway tree. At this point, air has already reached the state at which it enters the alveoli [2-3,5]. Thus, moisture transfer between the tissue and air was not considered as the air was assumed to have reached its saturation state prior to entering this region [5]. Accordingly, a transport equation to determine the mass fraction of vapour in the air was not required. Furthermore, the air temperature was held constant at body

temperature [2]. No thermal energy equation was used, as the temperature of the air and tissue were both assumed to be body temperature in the alveolar region. With no exchange occurring within the airway tree [9], the species concentrations of both oxygen and carbon dioxide were assumed to be equivalent to atmospheric air.

3.1.2 Oxygen Exchange

Atmospheric air is composed of many different gases, the most common being nitrogen, oxygen, carbon dioxide, and water vapour. As mentioned previously, air is fully saturated prior to reaching the alveoli [5]. The existence of water vapour within the alveolar air affects its density, as saturated air is denser than dry air at the same temperature. Therefore, a greater pressure will be required to move the air through the porous alveolar domain. However, the effects of this density change, between saturated and dry air, were neglected for this work, as the presence of water vapour within the air has little affect on species exchange within the alveoli. The present model considers three gases: nitrogen, oxygen and carbon dioxide. Nitrogen (N_2) is an inert gas, not absorbed by the lungs. Therefore the amount of nitrogen inhaled is equivalent to the amount exhaled. Like water vapour, nitrogen is a carrier.

As the purpose of this work was to determine a framework for simulating oxygen and carbon dioxide exchange within the lungs' alveoli, modelling species exchange was necessary. There are two accepted approaches for modelling species exchange; partial pressure difference and concentration difference. Both of these approaches have been used in previous studies [1-5,9,14,26]. These two approaches are interchangeable as partial pressure is directly related to mole fraction through

$$p = y_i P_{tot} \tag{3.1}$$

where p_i is the partial pressure of species i, y_i is the mole fraction of species i and P_{tot} is the total pressure of the mixture. Mole fraction is then directionally proportional to species concentration through

$$c_i = \frac{y_i}{\widehat{M}} \tag{3.2}$$

where c_i is the concentration of species i in mol/kg, y_i is the mole fraction of species i in the inhaled air and $\widehat{M}$ is the molar mass of the mixture in kg/mol. Therefore species exchange can be modelled with either parameter interchangeably. The concentration of oxygen in saturated air is used in the species transport equation for this work.

3.1.3 Carbon Dioxide Exchange

Modelling carbon dioxide exchange required a different approach. With oxygen concentration modelled with a species transport equation, the final concentrations of both oxygen and nitrogen were known values at every time step. The density of the air was assumed to be constant throughout the breathing cycle, making it possible to deduce the amount of carbon dioxide exchanged once the concentration of oxygen was known. Although this is not a perfect recreation of what occurs in vivo, for purposes of this work, it was deemed sufficient. The percent difference in the alveolar air density before and after exchange is less than one percent, so maintaining a constant air density for the model proposed in this work was accepted.

3.2 TRANSPORT EQUATIONS

The governing equations for airflow within the fluid domain are the instantaneous mass conservation, momentum and species transport equations given respectively as

$$\rho_f(\nabla \cdot \mathbf{u}) = 0 \tag{3.3}$$

$$\rho_f \left[\frac{\partial \mathbf{u}}{\partial t} + \nabla \cdot (\mathbf{u}\mathbf{u})\right] = -\nabla P + \mu \nabla^2 \mathbf{u} - \rho_f \mathbf{f} \tag{3.4}$$

$$\frac{\partial c_A}{\partial t} + \nabla \cdot (c_A \mathbf{u}) = D_f \nabla^2 c_A \tag{3.5}$$

where ρ_f is the density of the fluid, **u** is the velocity of the fluid, P is the pressure, c_A is the concentration of species A in moles per kg of the mixture, and D_f is the diffusion coefficient of species A in the fluid. These equations are solved directly in the fluid region, but must be volume-averaged to make them relevant in the porous region.

3.3 VOLUME-AVERAGING

Presently, porous media models are used for a variety of simulations involving heat and mass transfer. In such models, the method of volume averaging is used to integrate the general transport equations governing the flow and species transport over the porous media to produce a new set of governing equations for the averaged fields.

When developing a three-dimensional finite-volume CFD model for solving flows involving porous media, all equations must be volume-averaged. Volume averaging is used instead of solving for the individual flow fields through any one path of the porous structure. Instead, the fluid equations are solved in the average sense over each finite volume. This procedure is fully described by Betchen et al [8]. The following figure represents the cross sectional area of an idealized porous medium with the relevant nomenclature.

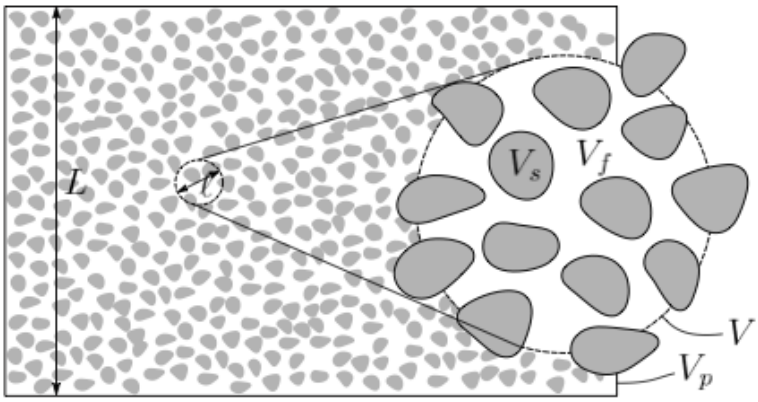

Figure 3.1. *A cross section of an averaging volume V, containing both solid and fluid constituents, V_s and V_f respectively. The length scale of the averaging volume, l is given in comparison to the length scale, L, of the porous domain, V_p [27].*

There are three different ways to volume average a property. The superficial or extrinsic average of property φ_i is given by

$$\langle \varphi_i \rangle = \frac{1}{\mathrm{V}} \int_{\mathrm{V}_i} \varphi_i \mathrm{dV} \tag{3.6}$$

This represents the average of property φ within constituent i when V_i represents the volume of constituent i within V and V represents the total volume of both constituents together. The intrinsic average is defined as

$$\langle \varphi_i \rangle^i = \frac{1}{\mathrm{V}_i} \int_{\mathrm{V}_i} \varphi_i \mathrm{dV} \tag{3.7}$$

The intrinsic and extrinsic averages are related by the porosity $\varepsilon = V_f/V$, yielding

$$\langle \varphi_f \rangle = \varepsilon \langle \varphi_f \rangle^f \tag{3.8}$$

for the fluid constituent and

$$\langle \varphi_s \rangle = (1-\varepsilon) \langle \varphi_s \rangle^s \tag{3.9}$$

for the solid constituent [29]. Therefore the total average of a desired property φ over a specified volume V is given by

$$\langle \varphi \rangle = \frac{1}{\mathrm{V}} \int_{\mathrm{V}} \varphi \mathrm{dV} \tag{3.10}$$

When volume averaging, two important rules should be noted. The spatial averaging theorem [28] is

$$\langle \nabla \varphi_f \rangle = \nabla \langle \varphi_f \rangle + \frac{1}{V} \int_{A_{fs}} \mathbf{n}_{fs} \varphi_f dA \tag{3.11}$$

and averaging theorem [28] is

$$\langle \nabla \cdot \mathbf{u} \rangle = \nabla \cdot \langle \mathbf{u} \rangle + \frac{1}{V} \int_{A_{fs}} \mathbf{n}_{fs} \cdot \mathbf{u} dA \tag{3.12}$$

The decomposition of property φ_i is given by

$$\varphi_i = \langle \varphi_i \rangle^f + \widetilde{\varphi}_i \tag{3.13}$$

where $\langle \varphi_i \rangle^f$ is the intrinsic average of φ_i in the fluid constituent and $\widetilde{\varphi}_i$ is the spatial deviation of φ_i.

3.4 MASS AND MOMENTUM EQUATIONS

The in house code used in this model already solved the mass and momentum equations [8]. The volume-averaging and coupling of the mass and momentum equations was completed by Betchen et al [8] and was not part of the present study, however it is briefly discussed here to see the context of where the species transport equation was implemented.

3.4.1 Volume-Averaged Mass Conservation Equation

This equation is used to represent the conservation of mass throughout the porous domain ensuring that the fluid entering the domain is equivalent in mass to the fluid exiting the domain. As this work used a rigid porous media model, it was important to properly conserve the mass of the air passing through the region of study. The conservation of mass prior to volume averaging is

$$\rho_f (\nabla \cdot \mathbf{u}) = 0 \tag{3.14}$$

while the extrinsic average of Eq. 3.14 expressing the volume-averaged mass conservation equation is

$$\rho_f (\nabla \cdot \langle \mathbf{u} \rangle) = 0 \tag{3.15}$$

where $\langle \mathbf{u} \rangle$ is the free channel velocity.

3.4.2 Volume-Averaged Momentum Equation

The equation used to calculate the momentum of a fluid passing through a pure fluid region is

$$\rho_f \left[\frac{\partial \mathbf{u}}{\partial t} + \nabla \cdot (\mathbf{uu})\right] = -\nabla P + \mu \nabla^2 \mathbf{u} - \rho_f \mathbf{f} \tag{3.16}$$

where μ is the dynamic viscosity of the fluid, kg/m·s, and $\mathbf{f}$ is the body force per unit mass, m/s^2. Assuming a constant porosity while being subject to length constraints, the intrinsic volume-averaged momentum equation becomes

$$\begin{aligned} \frac{\rho_f}{\varepsilon}\frac{\partial \langle \mathbf{u} \rangle}{\partial t} + \frac{\rho_f}{\varepsilon^2}\nabla \cdot (\langle \mathbf{u} \rangle \langle \mathbf{u} \rangle) = -\nabla \langle P \rangle^f + \frac{\mu}{\varepsilon}\nabla^2 \langle \mathbf{u} \rangle - \frac{\mu}{K}\langle \mathbf{u} \rangle \\ - \frac{\rho_f C_E}{\sqrt{K}} |\langle \mathbf{u} \rangle| \langle \mathbf{u} \rangle + \rho_f \mathbf{f} \end{aligned} \tag{3.17}$$

where ε is the porosity and K is the permeability. However the extrinsic average used by Betchen et al [8] is:

$$\begin{aligned} \rho_f \frac{\partial \langle \mathbf{u} \rangle}{\partial t} + \frac{\rho_f}{\varepsilon}\nabla \cdot (\langle \mathbf{u} \rangle \langle \mathbf{u} \rangle) = -\varepsilon \nabla \langle P \rangle^f + \mu \nabla^2 \langle \mathbf{u} \rangle - \frac{\varepsilon \mu}{K}\langle \mathbf{u} \rangle \\ - \frac{\varepsilon \rho_f C_E}{\sqrt{K}} |\langle \mathbf{u} \rangle| \langle \mathbf{u} \rangle + \varepsilon \rho_f \mathbf{f} \end{aligned} \tag{3.18}$$

The Darcy and the Forchheimer terms are both drag terms adding an additional resistance to the flow through the porous medium. The Darcy term, the third term on the right side of Eq. 3.18, dominates for low Reynolds numbers. The fourth term on the right hand side of Eq. 3.18, the Forchheimer term, takes inertia into account at higher Reynolds numbers.

3.5 OXYGEN TRANSPORT EQUATION

Introducing species transport into a porous medium has been done before [23-26] for various purposes. The following section describes how oxygen exchange was included in the existing 3D conjugate code [8].

3.5.1 Composition-Concentration Conversion

Inhaled gas measurements are given in percent composition [4,7], also known as mole fraction, and can be used to calculate the partial pressure and concentration of the individual components. Although most lung models use partial pressure as the driving

force of exchange [1-5,8], the volume averaged exchange equations used in previous studies [23-26,28] use species concentration as the driving force for exchange. Therefore, the inhaled gas compositions required conversion into concentration values with the unit moles of oxygen per mixture mass (kg) before being solved in the transport equation. By treating air as an ideal gas, the concentration of the air's individual constituents could be determined using Eq. 3.2.

3.5.2 Volume-Averaged Species Transport Equation Fluid Constituent

The original form of the species transport equation for the fluid constituent given by Whitaker [28] is

$$\frac{\partial c_A}{\partial t} + \nabla \cdot (c_A \mathbf{u}) = D_f \nabla^2 c_A \tag{3.19}$$

Please note the process for volume-averaging the species transport equation used here was taken from Whitaker [28].

The first step required to volume-average Eq. 3.19 is to take the superficial or extrinsic average of the equation

$$\langle \frac{\partial c_A}{\partial t} \rangle + \langle \nabla \cdot (c_A \mathbf{u}) \rangle = \langle D_f \nabla^2 c_A \rangle \tag{3.20}$$

The first term of Eq. 3.20 becomes

$$\langle \frac{\partial c_A}{\partial t} \rangle = \frac{\partial \langle c_A \rangle}{\partial t} \tag{3.21}$$

with the assumption that the integration region does not change with respect to time [29]. Using the averaging theorem, Eq. 3.12, the second term of Eq. 3.20 can be changed to

$$\langle \nabla \cdot (c_A \mathbf{u}) \rangle = \nabla \cdot \langle c_A \mathbf{u} \rangle + \frac{1}{V} \int_{A_{fs}} \mathbf{n}_{fs} \cdot (c_A \mathbf{u}) \, dA \tag{3.22}$$

where $\mathbf{n}_{fs}$ is the unit-normal vector directed from the fluid to solid constituent and A_{fs} is the interface between the fluid and solid constituents, m^2. When considering a no-slip

boundary condition at the surface between the two constituents of the porous medium the integral term of Eq. 3.22 is equivalent to zero simplifying the equation to

$$\langle \nabla \cdot (c_A \mathbf{u}) \rangle = \nabla \cdot \langle c_A \mathbf{u} \rangle \tag{3.23}$$

The spatial decomposition of the right side of Eq. 3.23 is given by

$$\nabla \cdot \langle c_A \mathbf{u} \rangle = \varepsilon \langle \mathbf{u} \rangle^f \cdot \nabla \langle c_A \rangle^f + \nabla \cdot \langle \tilde{\mathbf{u}} \tilde{c}_A \rangle \tag{3.24}$$

Modifying the term on the right side of Eq. 3.20 using the averaging theorem yields

$$\langle D_f \nabla^2 c_A \rangle = D_f \nabla \cdot \langle \nabla c_A \rangle + \frac{1}{V} \int_{A_{fs}} \mathbf{n}_{fs} \cdot D_f \nabla c_A dA \tag{3.25}$$

Using the averaging theorem again yields

$$\langle D_f \nabla^2 c_A \rangle = D_f \nabla \cdot \left[\nabla \langle c_A \rangle + \frac{1}{V} \int_{A_{fs}} \mathbf{n}_{fs} c_A dA \right] + \frac{1}{V} \int_{A_{fs}} \mathbf{n}_{fs} \cdot D_f \nabla c_A dA \tag{3.26}$$

Although by assuming that the concentration of species A, c_A, at the interface between the fluid and solid constituents, A_{fs}, is constant, while taking the decomposition of the concentration term from Eq. 3.13, results in

$$\frac{1}{V} \int_{A_{fs}} \mathbf{n}_{fs} \tilde{c_A} dA = 0 \tag{3.27}$$

creating

$$\langle D_f \nabla^2 c_A \rangle = D_f \varepsilon \nabla^2 \langle c_A \rangle^f + \frac{1}{V} \int_{A_{fs}} \mathbf{n}_{fs} \cdot D_f \nabla c_A dA \tag{3.28}$$

Combining Eqs. 3.21, 3.24 and 3.28 gives the volume-averaged version of the species transport equation, Eq. 3.20, in the fluid region as

$$\varepsilon \frac{\partial \langle c_A \rangle^f}{\partial t} + \varepsilon \langle \mathbf{u} \rangle^f \cdot \nabla \langle c_A \rangle^f = D_f \varepsilon \nabla^2 \langle c_A \rangle^f + \frac{1}{V} \int_{A_{fs}} \mathbf{n}_{fs} \cdot D_f \nabla c_A dA - \nabla \cdot \langle \tilde{\mathbf{u}} \tilde{c}_A \rangle \tag{3.29}$$

which is the intrinsic form of Whitaker's [28] final volume-averaged species transport equation. Note the first term of Eq. 3.29 was changed from the explicit form to the implicit form using Eq. 3.8. Assuming the Reynolds number approaches zero once air reaches the terminal alveoli (due to the very low velocity at this point) results in

$$\nabla \cdot \langle \tilde{\mathbf{u}} \tilde{c}_A \rangle = 0 \tag{3.30}$$

So the volume-averaged species transport equation for the fluid constituent becomes

$$\varepsilon \frac{\partial \langle c_A \rangle^f}{\partial t} + \langle \mathbf{u} \rangle \cdot \nabla \langle c_A \rangle^f = D_f \varepsilon \nabla^2 \langle c_A \rangle^f + \frac{1}{V} \int_{A_{fs}} \mathbf{n}_{fs} \cdot D_f \nabla c_A dA \tag{3.31}$$

The final term in Eq. 3.31 is the interfacial absorption term. This can be approximated using

$$\frac{1}{V} \int_{A_{fs}} \mathbf{n}_{fs} \cdot D_f \nabla c_A dA = -K_{eq} \frac{A_{fs}}{V} \frac{\partial \langle c_A \rangle^f}{\partial t} \tag{3.32}$$

where K_{eq} is the absorption coefficient, D_f represents the diffusion coefficient for species A within the fluid constituent in m^2/s, c_A represents the molar concentration of species A per mixture mass mol/kg, A_{fs} is the area of the interface within a control volume in m^2 and V is the volume of a control volume m^3 [28]. This interfacial absorption term uses the change in concentration gradient over time to control the amount of species A being absorbed by the solid constituent, therefore removing it from the fluid. This does not consider an existing concentration of species A at the wall of the solid constituent. The specific surface area of the porous medium is given as $a_{fs} = A_{fs}/V$ and has units m^2/m^3.

Therefore the final volume-averaged transport equation for the fluid phase of the porous domain is

$$\varepsilon \frac{\partial \langle c_A \rangle^f}{\partial t} + \langle \mathbf{u} \rangle \cdot \nabla \langle c_A \rangle^f = D_f \varepsilon \nabla^2 \langle c_A \rangle^f - K_{eq} \frac{A_{fs}}{V} \frac{\partial \langle c_A \rangle^f}{\partial t} \tag{3.33}$$

The absorption coefficient K_{eq} needs to be determined before this equation can be solved. It is necessary to determine whether the absorption term described by Whitaker [28], remains valid when modelling gaseous exchange in the lungs. Therefore, a better

understanding about the time scale of oxygen diffusion through the alveolar air compared to the time scale of respiration is needed. The conditions needing to be modelled with the volume averaged oxygen transport equation can be confirmed with additional knowledge regarding the absorption within each alveolus.

3.5.3 Volume-Averaged Species Transport Equation Solid Constituent

The original form of the species transport equation for the solid constituent is equivalent to the fluid constituent [28] without the convective term,

$$\frac{\partial c_A}{\partial t} = D_f \nabla^2 c_A \tag{3.36}$$

which can be volume-averaged in the same way the fluid constituent equation was volume-averaged. This leads to the flowing volume-averaged intrinsic concentration equation

$$(1-\varepsilon)\frac{\partial \langle c_A \rangle^s}{\partial t} = D_s(1-\varepsilon)\nabla^2 \langle c_A \rangle^s - K_{eq}\frac{A_{fs}}{V}\frac{\partial \langle c_A \rangle^s}{\partial t} \tag{3.37}$$

for the solid constituent. However, the absorption term is still listed as a function of time. Therefore, understanding the time scale of the transport within the solid is also important for the closure of this equation. Again, this must be verified through the pore level simulations discussed in Chapter 4.

3.6 CARBON DIOXIDE EXCHANGE

As explained in Section 3.1.3, carbon dioxide exchange is determined once the final value of oxygen concentration is known. A crude approximation for the amount of carbon dioxide absorbed is to maintain a constant density and simply replace the depleted oxygen.

3.6.1 Concentration-Composition Conversion

Once oxygen exchange has occurred, the exhaled air leaves the porous domain. By rearranging Eq. 3.2, the mole fractions of the exhaled air can be determined for both oxygen and nitrogen by

$$y_i = c_i \widehat{M} \tag{3.40}$$

where y_i is the mole fraction of the constituent i, c_i concentration of constituent i in mol/kg and $\widehat{M}$ is the molar mass of the mixture in kg/mol. However, the volume-averaged concentration of both nitrogen and oxygen are given per control volume, therefore in order to use Eq. 3.40, the average of both concentrations needed to be determined along the outlet. To increase the accuracy of the model, a different molar mass of the mixture was used. When the initial concentrations of oxygen and nitrogen were determined, the molar mass of dry atmospheric air was used. However, once air is exhaled, the molar mass has changed due to the composition changes imposed by the species exchange within the alveoli. Therefore, to return the concentration values of oxygen and nitrogen along the outlet to mole fractions, the molar mass of exhaled air was used. This would better estimate the changes in composition occurring within the region of study. The mole number of nitrogen would not have changed, as this gas is a carrier and no exchange occurs between it and the tissue.

3.6.2 Carbon Dioxide Exchange

With known mole fractions of both oxygen and nitrogen at the outlet, the remainder is composed of carbon dioxide

$$y_C = 1.0 - y_O - y_N \tag{3.41}$$

where y_C is the mole fraction of carbon dioxide exchanged in the alveoli prior to being exhaled.

3.7 DISCRETIZATION OF THE VOLUME-AVERAGED EQUATIONS

The volume-averaged mass, momentum and oxygen transport equations need to be discretized over the domain before they can be solved. Betchen et al [8] discretized these equations using a collocated finite volume framework integrated over a control volume. The discretized equations are given for the mass, momentum and generalized transport equations respectfully,

$$\sum_i \dot{m}_i = 0 \tag{3.42}$$

$$\frac{\rho_f V_p\left(\mathbf{u}_p - \mathbf{u}_p^o\right)}{\Delta t} + \sum_i \dot{m}_i \left(\mathbf{u}_i - \mathbf{u}_p\right) = -V_p(\nabla P)_p + \sum_i \mu \left(A \frac{\partial \mathbf{u}}{\partial n}\right)_i + \rho_f V_p \mathbf{f}_p \tag{3.43}$$

$$\frac{\rho_f V_p c_{p,f}\left(\varphi_p - \varphi_p^o\right)}{\Delta t} + \sum_i \dot{m}_i \, c_{p,f}\left(\varphi_i - \varphi_p\right) = \sum_i D_f \left(A \frac{\partial \varphi}{\partial n}\right)_i \tag{3.44}$$

where i = 1,2,…, N, are evaluated at the integration point at the centroid of face i [8]. As this work dealt solely with porous domains, the discretized equations at the interfaces are not included here, simplifying the problem. The interpolation technique by Rhie et al [30] was used to maintain coupled pressure and velocity in the momentum equation.

The discretized versions of volume-averaged equations, Eqs. 3.15, 3.18, 3.34 and 3.38 are given by Betchen et al [8] as

$$\sum_i \dot{m}_i = 0 \tag{3.45}$$

$$\begin{aligned} &\frac{\rho_f V_p\left(\langle \mathbf{u} \rangle_p - \langle \mathbf{u} \rangle_p^o\right)}{\Delta t} + \sum_i \dot{m}_i \left(\frac{\langle \mathbf{u} \rangle_i}{\varepsilon} - \frac{\langle \mathbf{u} \rangle_p}{\varepsilon}\right) \\ &\qquad = -\varepsilon V_p (\nabla \langle P \rangle^f)_p + \sum_i \mu \left(A \frac{\partial \langle \mathbf{u} \rangle}{\partial n}\right)_i - \frac{\varepsilon V_p \mu_f}{K} \langle u \rangle_p \\ &\qquad - \frac{\varepsilon \rho_f V_p c_E}{\sqrt{K}} \left|\langle \mathbf{u} \rangle_p\right| \langle \mathbf{u} \rangle_p + \rho_f V_p \mathbf{f}_p \end{aligned} \tag{3.46}$$

$$\frac{\varepsilon\rho_f V_p c_{p,f}\left(\langle\varphi_f\rangle_p^f - \langle\varphi_f\rangle_p^{f,o}\right)}{\Delta t} + \sum_i \dot{m}_i\, c_{p,f}\left(\langle\varphi_f\rangle_i^f - \langle\varphi_f\rangle_p^f\right) = \sum_i \left(D_{fe} A \frac{\partial\langle\varphi_f\rangle^f}{\partial n}\right)_i + kA_{sf}V_p\left(\langle\varphi_s\rangle_p^s - \langle\varphi_f\rangle_p^f\right) \tag{3.47}$$

$$\frac{(1-\varepsilon)\rho_s V_p c_s\left(\langle\varphi_f\rangle_p^s - \langle\varphi_f\rangle_p^{s,o}\right)}{\Delta t} = \sum_i \left(D_{se} A \frac{\partial\langle\varphi_s\rangle^s}{\partial n}\right)_i - kA_{sf}V_p\left(\langle\varphi_s\rangle_p^s - \langle\varphi_f\rangle_p^f\right) \tag{3.48}$$

where

$$\dot{m}_i = \rho_f A_i(\langle\hat{\mathbf{u}}\rangle_i \cdot \mathbf{n}) \tag{3.49}$$

is the mass flow rate [8]. Results for the porous plug flow test case can be found in Appendix A.1. The central differencing scheme (CDS) was used for these simulations to approximate the integration point values for the advection terms using the neighbouring cells.

3.8 REQUIREMENTS FROM PORE LEVEL SIMULATIONS

It is important to know if the application of engineering models to biological phenomena is appropriate, and whether respiration can be properly simulated using the engineering techniques discussed in this chapter. The effects of the oxygen transport properties of the air and tissue need to be determined before the species exchange can be modelled with the volume-averaged oxygen transport equation. Without a clear understanding of the biological process within the terminal alveoli, the absorption term can not be closed and it is unable to replicate the alveolar exchange.

Pore level simulations are needed to elucidate how the oxygen transport properties of the air and lung tissue affect the resistance to diffusion and, therefore, the total amount of oxygen absorbed by the alveoli. Examining previous literature of terminal alveolated clusters yielded no oxygen exchange results. Previous studies [19-21] focused on airflow

without studying species exchange. Therefore, pore level simulations were completed to determine the relationship between the time scale of oxygen diffusion and the time scale of respiration. These simulations will reveal whether the resistance to oxygen absorption is dependent upon the transport properties of the alveolar air or the lung tissue. Once this is known, the absorption term can be closed and the volume-averaged oxygen transport equations introduced in this chapter can be used to solve alveolar oxygen exchange in the porous domain as a function of the correct parameters.

CHAPTER 4

PORE LEVEL SIMULATIONS

Pore level simulations were required to elucidate the relationship between the time scale of oxygen diffusion and the time scale of respiration. The volume-averaged oxygen transport equations introduced in Chapter 3 require closure to replicate alveolar species exchange. Modelling the absorption term between the air and the tissue is reliant upon correctly simulating the resistance caused by the transport properties of the air and the lung tissue. Therefore, an idealized model of a terminal alveolated cluster was developed to mimic the functionality of a real acinar cluster without simulating the resistance to diffusion in the tissue. The results given in this chapter reveal that the transport properties of the air allow the maximum amount of oxygen to be diffused to the tissue regardless of respiration frequency, therefore the resistance to oxygen diffusion in the closure term must be simulated using the transport properties of the tissue. As no previous literature exists for models studying oxygen concentration at the alveolar level, additional studies were completed to validate the transport results given here.

4.1 MODEL DEVELOPMENT

Developing an appropriate model for the required pore level simulations was completed in stages to ensure the greatest accuracy. These stages are discussed in detail throughout the following sections along with how spatial and temporal independence were achieved for the simulations.

4.1.1 Geometry Development

In order to capture the biological process as closely as possible, realistically mimicking the alveolar geometry is crucial. However, this is often not possible, so idealized geometries are used instead. Idealizing the geometry of a terminal acinar cluster for

modelling purposes has been done various ways based on different interpretations of histological images [19-21]. The geometric models used in other studies were validated using different images, with the assumptions changing depending on their expected results. It can easily be determined by examining an image of the lungs' alveoli that no solid walled duct can be seen, with individual alveoli attached, amongst the porous geometry of the alveoli. The only solid walled duct present in Figure 2.1 feeds into the alveolated ducts with no spaces present between the alveoli. These ducts have alveoli on all sides and must expand along with them during inhalation. Therefore the geometry proposed by Harding et al [19] (refer to Figure 4.1) was not considered as their use of a rigid solid walled terminal bronchiole surrounded by equally spaced non-interacting spherical alveoli was deemed inconsistent with the goals of this work. This geometry includes no alveolar septa [31] and considers alveolar expansion to be unhindered by surrounding alveolated clusters. Therefore, although this geometry could produce closure parameters, these parameters would not be correct for the current work, as the acinar clusters were not designed to nestle together like those seen in Figure 2.1.

Figure 4.1. *Replication of the geometry proposed by Harding et al [19] showing the spherical expanding non-interacting alveoli around the central rigid duct.*

The geometry proposed by Kumar et al [20] is based on geometric data from Weibel et al [31]. They assume alveoli are closely packed with no space between them, expanding along with the terminal bronchiole. The shape of each idealized alveolus is a truncated octahedron, which can be visualized by removing a four-sided triangular prism from the

corners of an octahedron. When assembled about a duct, this shape allows for the alveoli to nestle together whilst creating an axis symmetric geometry. Consequently, if many of these terminal regions were assembled together and sliced in half to view the internal structure, it would resemble a porous geometry. Therefore, the geometry developed by Kumar et al [20] was replicated for this work as it was deemed more geometrically accurate for the requirements of the pore level simulations.

The geometry proposed by Kumar et al [20] was replicated using SolidWorks® 2012. Each alveolus was assembled onto the base duct to maintain the required geometry. The acinar region used for these simulations consisted of 22 alveoli surrounding a central terminal bronchiole. Figure 4.2 shows a representation of the geometry used with the duct and terminal alveolus both visible. The porous structure of the interacting alveoli has been maintained without compromising the function of the terminal cluster.

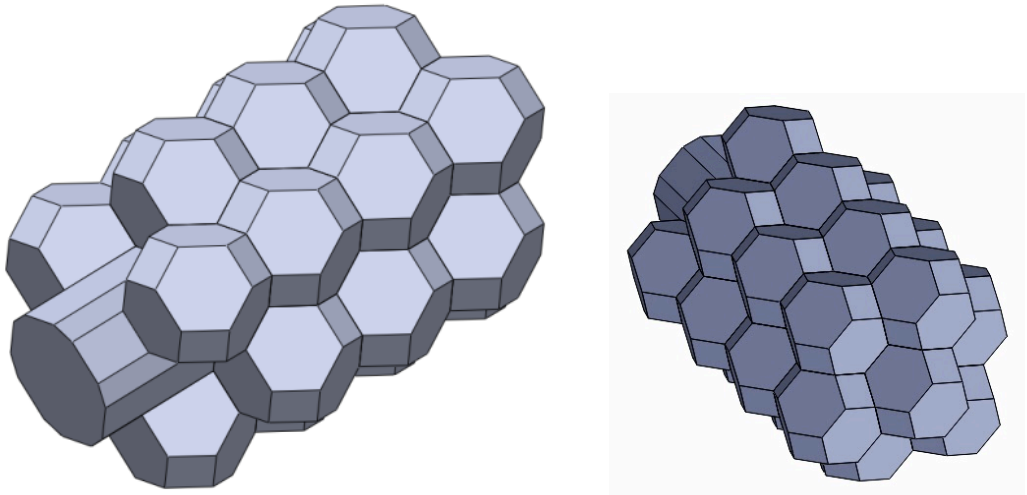

(a) *(b)*

Figure 4.2. *The truncated octahedron terminal duct geometry with 22 alveoli used for the pore level simulations based on the geometry proposed by Kumar et al [20] (a) front view with the duct visible and (b) rear view showing the terminal alveolus.*

The size on an alveolus hardly changes across different lung specimens [32]. Ochs et al [32] measured the number-weighted mean volume of an alveolus as 4.2×10^6 μm^3 with a total observation variation of 10%. They determined while the size of the lung affects its total volume, the average size of an alveolus is not related to the size of the lung.

Therefore, larger lungs contain more alveoli than smaller lungs. Approximating each alveolus with the same dimensions, regardless of its location along the terminal bronchiole, was deemed sufficient for this work.

4.1.2 Meshing

Before a mesh could be developed in ANSYS ® ICEM, the imported geometry required some modification. All internal duct walls were removed to allow for airflow between the duct and the alveoli. Internal walls were included to maintain the existence of the walls between the alveoli. This ensured the air could not pass directly from one alveolus to another, only from the duct to an alveolus.

4.2 BOUNDARY AND INITIAL CONDITIONS

The boundary conditions applied to the terminal acinar cluster should mimic the conditions present within the lung during respiration. The initial values were set to the conditions at the end of the previous exhalation. This will be discussed in further detail in the following sections.

4.2.1 Mass and Momentum Equation

To properly simulate the moving domain of a terminal acinar cluster an assumed volume expansion of 15% was modelled. This expansion factor was calculated for a 500 ml tidal volume with a 4.5 L lung capacity with approximately 80-90% of the volume stored in the alveoli, corresponding with normal breathing [18]. With the centre of the inlet/outlet placed on the software's origin, the walls were expanded by

$$x = initcartcrd\_x * (1 + A * sin(\omega * t)) \quad (4.1a)$$

$$y = initcartcrd\_y * (1 + A * sin(\omega * t)) \quad (4.1b)$$

$$z = initcartcrd\_z * (1 + A * sin(\omega * t)) \quad (4.1c)$$

where x, y and z are the new Cartesian coordinates of mesh displacement, $initcartcrd\_x$, $initcartcrd\_y$ and $initcartcrd\_z$ are the old Cartesian coordinates of x, y and z, A is the amplitude of 0.0228 for 15% expansion, ω is the angular frequency of respiration (i.e. 1.25664 rad/s was used for one breath every five seconds) and t is the current time. By defining the expansion of the mesh it was not necessary to define velocity boundary conditions on the inlet. However the velocity of the air at the alveolar walls was set to zero with a no slip condition. The pressure was defined at the inlet with a relative pressure of 0 Pa. The velocity and pressure values were initialized throughout the domain to zero in all directions. Changing the frequency of respiration and the tidal volume expansion was possible by changing ω and A in the mesh displacement equations.

4.2.2 Oxygen Transport Equation

Determining the boundary and initial conditions for the oxygen transport equation was more complex than the velocity and pressure conditions. The oxygen transport equation, Eq. 3.5, required the oxygen concentration to have the units of moles oxygen per kg mixture. The inlet condition was set to the oxygen concentration of atmospheric air. This was possible as no exchange occurs prior to oxygen reaching the alveoli [9], making the atmospheric boundary condition valid at the inlet of the terminal cluster studied in this work. The oxygen concentration at the inlet, calculated using Eq. 3.2, was found to be 7.279 mol/kg. The concentration of the oxygen at the walls was also found using Eq. 3.2, however the molar mass of the mixture was calculated using the gaseous mole fractions of exhaled air. Therefore the lowest possible exhaled oxygen concentration would be the expected value determined experimentally [4]. The concentration of oxygen at the walls was 5.514 mol/kg, consistent with the exhaled concentration of oxygen and the final concentration of oxygen within the oxygenated blood leaving the lungs. The short duct leading into the alveolar cluster seen in Figure 4.2a, was given a no flux boundary condition to account for no oxygen exchange across the duct walls prior to reaching the alveoli [9]. The oxygen concentration of the domain was initialized with the same concentration as the walls, 5.514 mol/kg. This initial value was selected as though the first breath cycle were occurring directly after a previous breath. The oxygen

concentration within the cluster would be equivalent to the concentration at the wall as all oxygen inhaled in the previous breath would either have been absorbed or exhaled.

4.2.3 Other Parameters

The pore level simulations were run isothermally as no temperature differences are present between the air and the alveolar walls [2]. The kinematic diffusivity was set to 2.0×10^{-5} m^2/s, the accepted value for the diffusivity of oxygen in air.

4.3 SPATIAL AND TEMPORAL INDEPENDENCE

To ensure the results were both grid independent and time independent, simulations were run using different grid sizes and different time intervals. These independence simulations were run over 5 breaths at a frequency of 0.2 Hz, regular resting respiration. Therefore 25 seconds of real time were simulated. The three different grid sizes tested were course, fine and ultrafine at 366,774, 606,466 and 985,882 tetrahedral volumes respectively. Two different time intervals were also tested: 100 time steps (Δt = 0.25s) and 200 time steps (Δt = 0.125s) per breath cycle. Therefore a total of six simulations were conducted to assess spatial/temporal independence. To compare the independence across these simulations, the amount of oxygen absorbed by the cluster per breath was compared for the last simulated breath. This was calculated by comparing the total amount of oxygen that entered the cluster through the inlet with the total amount of oxygen that exited the cluster though the same boundary. The percent difference was very small across the six simulations however the ultrafine grid size of 985,882 volumes took twice as long to run a five-breath simulation than the fine grid of 606,466 volumes. Therefore the percent differences between the course and fine meshes were examined to decrease computational time. The percent difference of 0.0007% between the course and fine meshes and time steps was very small and considered negligible. However to increase the accuracy of the results the fine mesh with 606,466 volumes over 200 times steps per breath cycle was selected for all further simulations. Figure 4.3 represents the final mesh.

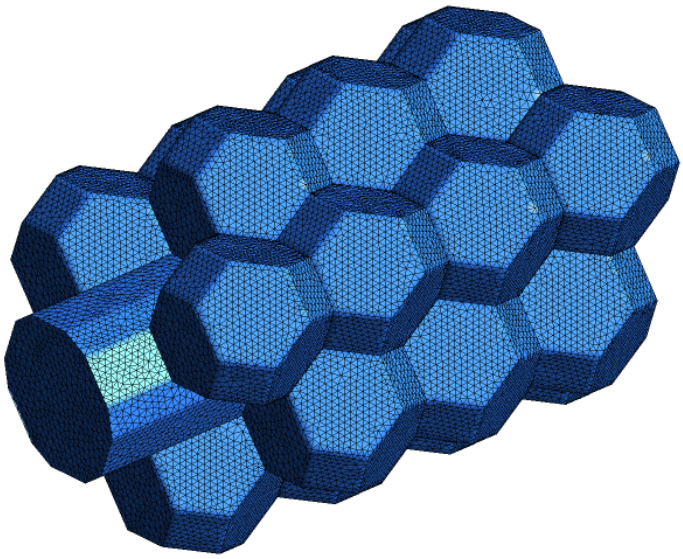

Figure 4.3. *The final mesh of 606,466 tetrahedral elements used to achieve spatial independence with 200 time steps per breath cycle to achieve temporal independence.*

4.4 RESULTS

The purpose of these pore level simulations was to gain a better understanding of the oxygen exchange occurring on the alveolar level. Determining how oxygen is transported from the inlet of the cluster to the tissue is important to comprehend the time scale of oxygen diffusion through the air versus the time scale of respiration. This is needed to close the volume-averaged oxygen transport equation and to determine the average exchange coefficient for the terminal cluster.

Before the results are given, it should be noted the resistance to diffusion from the alveolar air to the tissue is not modelled here. Therefore, any oxygen transported to the alveolar walls will be absorbed directly into the tissue. These results are only valid for the potential transport of oxygen through the alveolar air. The transport properties of the tissue will be discussed in Chapter 5.

4.4.1 Pressure Results

Due to the complex geometry of the terminal cluster, before the oxygen transport through the alveolar air can be studied, the velocity and the pressure distributions needed to be fully understood. Negative pressure breathing results from the diaphragm dropping, causing the volume of the lungs to increase, resulting in a decrease in the internal lung pressure. This pressure decrease causes inhalation by drawing air into the lungs to equalize the pressure difference. When the diaphragm moves upwards again the lungs are compressed, increasing the internal pressure above atmospheric, resulting in the exhalation of the inhaled air. With mesh motion defined for the pore level simulations, the resulting pressure changes should match those observed in vivo. Figure 4.4 plots the gauge pressure of the terminal cluster at four separate time frames during the last breath cycle.

At the beginning of both exhalation and inhalation the gauge pressure in the alveolar cluster is close to zero. Therefore the pressure is atmospheric in the cluster. However once the cluster begins to expand the pressure decreases, drawing air into the alveoli. This can be seen in Figure 4.4b with the drop in alveolar pressure. During exhalation as the alveolar cluster decreases in volume again, the pressure increases above atmospheric, forcing the air out. Figure 4.4d represents the alveolar pressure during the middle of the exhalation.

The changes in pressures observed during the simulation were very small, with a range of 1.537×10^{-3} Pa to -1.519×10^{-3} Pa. The simulated cluster is located at the terminal end of an approximately 20 level bifurcating airway tree. With each bifurcation, the pressure decreases due to the increase in the total area of the pathways. Once the terminal alveoli are reached, the pressure has decreased dramatically from the original pressure differences in the trachea. Therefore, the pressure differences simulated here appear to be reasonable within the confines of the geometry.

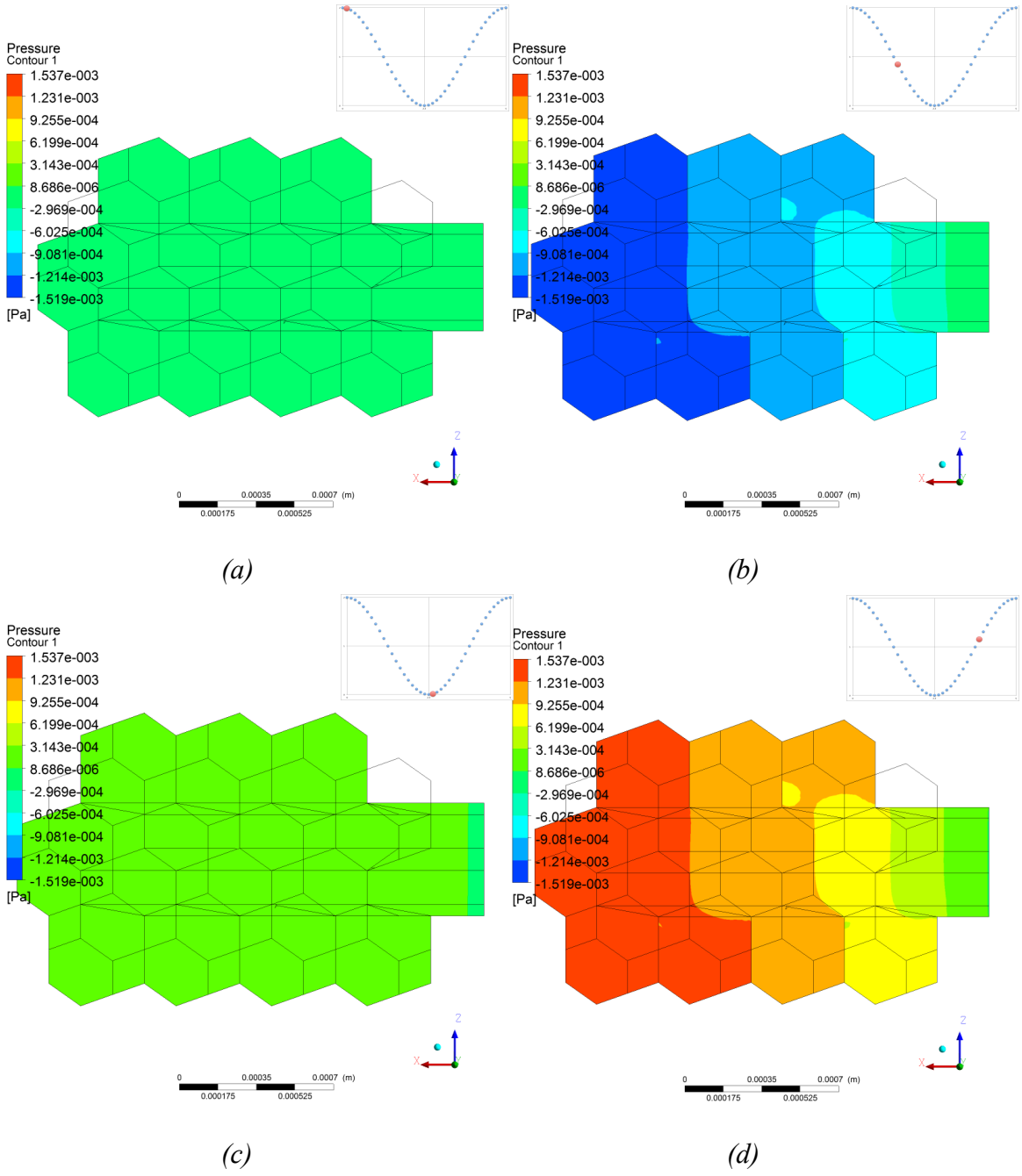

Figure 4.4. *The pressure contours have been plotted at the red time point seen in the breathing cycle in the upper right corner of each contour (a) the beginning of inhalation (b) the middle of inhalation (c) the beginning of exhalation and (d) the middle of exhalation. Note the extremes in pressure occur at the terminal end of the alveoli due to the mesh motion. These results were for 15% tidal volume expansion with a frequency of one breath every five seconds or 0.2 Hz. The units of these contours are Pa.*

4.4.2 Velocity Results

Closing the volume-averaged oxygen transport equation requires an understanding of the airflow in each alveolus. If the airflow differs within each alveolus, it will be necessary to perform an averaging over the 22 alveoli present in the model to properly determine the closure parameters.

With alveolar pressure driving the airflow within the terminal acinar cluster, the air motion should be reflective of this. The velocity contours of the airflow are plotted along with the velocity vectors at four states during the last breath cycle in Figure 4.5. These plots show almost no air motion between exhalation and inhalation, and vice versa, corresponding to the pause occurring at these points during a regular breathing cycle. When air reaches the terminal alveoli at the end of inhalation, the velocity of the air is small. The same pause happens at the end of exhalation, before the air changes direction again. The largest velocity magnitudes are present in the duct during the middle of inhalation and exhalation. These velocity contours and vectors can be seen in Figures 4.5b and 4.5d.

For regular resting respiration, the maximum airflow velocity was found to be 1.273×10^{-3} m/s when the diameter of the duct was 0.516 mm. The only comparable work by Harding et al [19] achieved maximum velocities of 9.3×10^{-4} m/s with a constant duct diameter of 0.23mm. The differences between the maximum velocity values can be attributed to the differences in geometry and tidal volume expansion. At thirteen alveoli, Harding et al [19] modelled half the number of alveoli simulated in this work. Their duct remained motionless while the alveoli expanded around it. Therefore, although never stated, the volume of their terminal alveolar cluster would have been smaller than the current study. The tidal volume expansion values for Harding et al [19] and the present work were 15.6% and 15% respectively; the lower velocity values measured by Harding et al [19] were likely the result of less volume moving through the cluster. However the magnitudes of the two maximum velocities are comparable, validating the results of the present simulation.

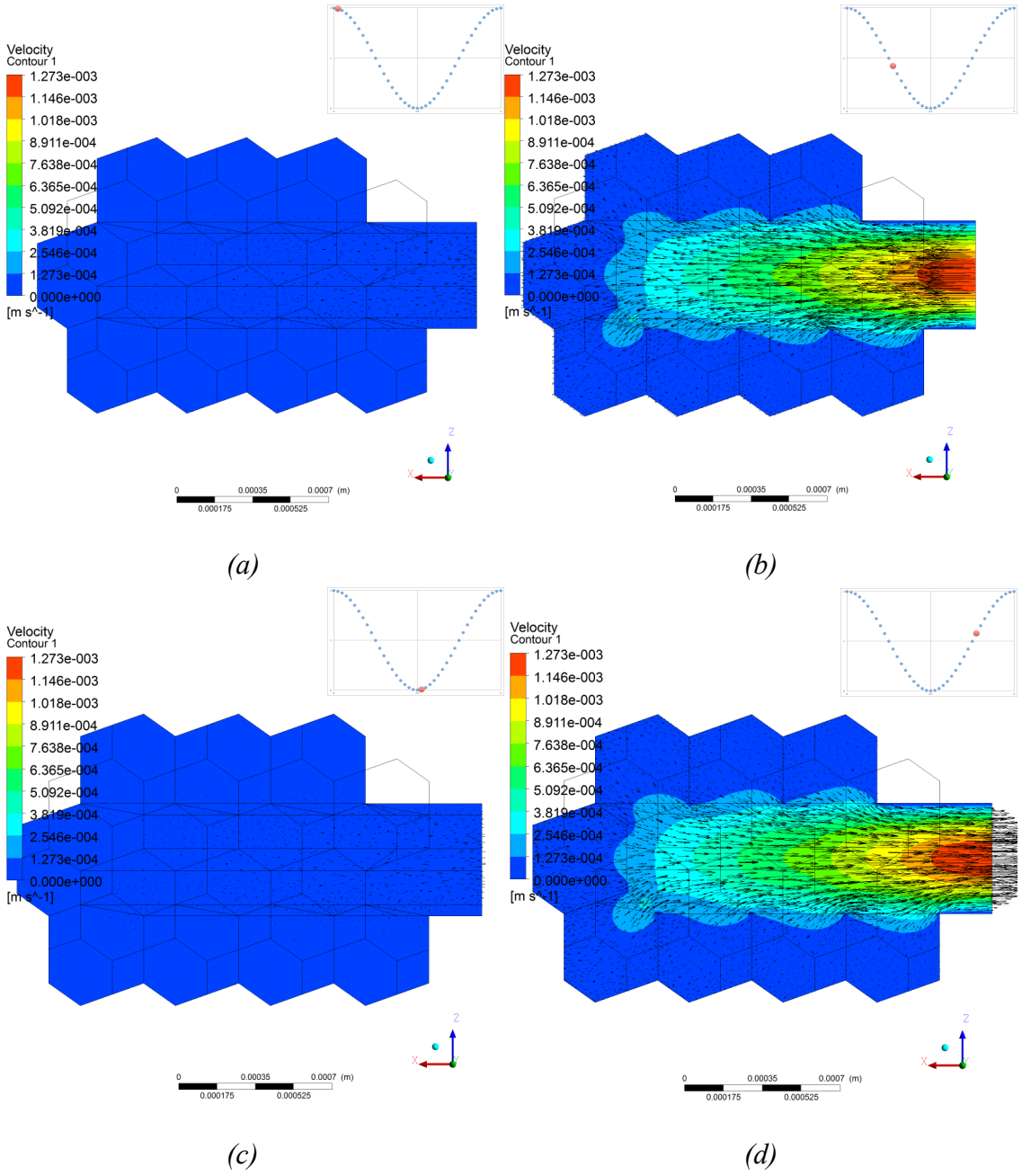

Figure 4.5. *The velocity contours plotted along with the vector diagrams at the red time point seen in the breathing cycle in the upper right corner of each contour same as the previous figure. At (b) and (d) the largest velocities are noted. These results were for 15% tidal volume expansion with a frequency of one breath every five seconds or 0.2 Hz. The units of these contours are m/s.*

Previous studies of terminal acinar clusters [19-21] found no regions of recirculation were present. Streamlines have been plotted in Figure 4.6 at the end of inhalation. No regions of recirculation are present within the alveolar domain studied in this work consistent with the previous studies [19-21]. The PIV study completed by Oakes et al [21] showed for a healthy simulated terminal cluster, fresh air penetrated approximately 63% into the cluster. During the present simulation the inhaled air did not penetrate the full length of the terminal cluster, consistent with Oakes et al [21]. Therefore fresh air does not fully penetrate the terminal cluster, and the air present in the duct at the end of the previous exhalation is the air drawn into the alveoli during the next inhalation. Therefore the fresh oxygen only reaches the terminal bronchiole, not the alveolar walls through advection alone. Oxygen can only reach the alveolar walls by diffusing through the stale air remaining within the alveoli.

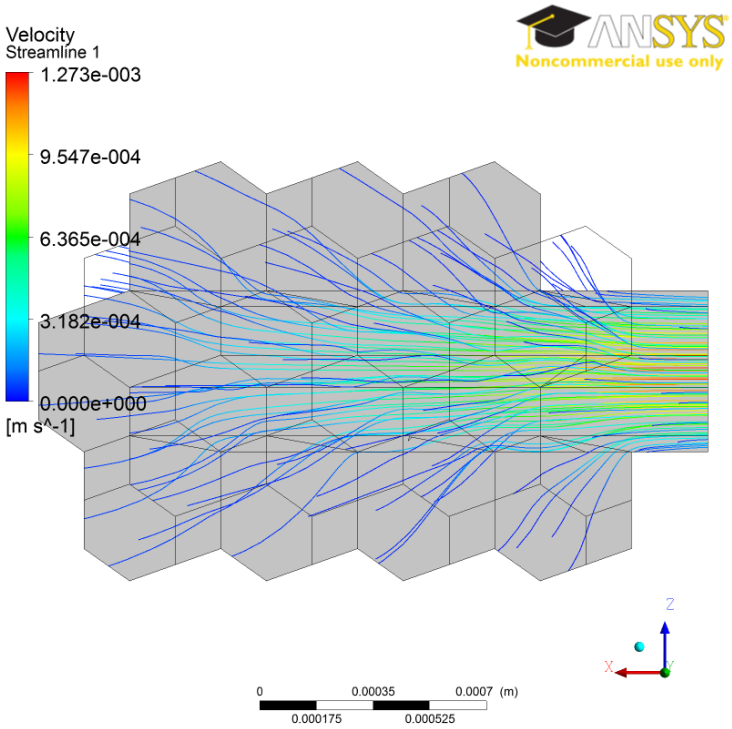

Figure 4.6. *The streamlines of the airflow in the terminal alveolated cluster. Note there are no regions of recirculation present. These results were for 15% tidal volume expansion with a frequency of one breath every five seconds or 0.2 Hz. The units of the streamlines are m/s.*

Another point of interest taken from the velocity results is each alveolus appears to experience the same velocity conditions as the ones around it. Kumar et al [20] noticed the asymmetry in the placement of the alveoli about the central axis did not result in any differences in the airflow patterns. This observation is consistent with the streamlines in Figure 4.6. Therefore each alveolus sees the same velocity conditions regardless of its location along the duct. This leads to the possibility no extra averaging will need to be completed for each alveolus along the terminal duct to determine the required closure parameters. This will be become more apparent in Section 4.4.3.

4.4.3 Oxygen Transfer Results

The oxygen transport simulations in the terminal acinar cluster were achieved through the use of the built in species transport equation of ANSYS® CFX, Eq. 3.5. With the airway tree volume consisting of approximately 10% of the lungs' total volume [18], a 15% tidal volume expansion would replace the airway tree with fresh oxygen. Figure 4.7 shows scaled oxygen concentration contours over selected time steps. The inlet was maintained at a constant oxygen concentration of 7.279 mol/kg during inhalation, corresponding to the oxygen concentration of atmospheric air. The values of oxygen concentration are shown for the low end of concentration (between 5.51397 mol/kg and 5.52 mol/kg) with the oxygen concentration at the wall defined as 5.514 mol/kg, or the concentration of oxygen in exhaled air. This scaling was completed so the oxygen concentration contours would be visible. At the beginning of inhalation, Figure 4.7a, the velocity is very low (refer to Figure 4.5a), however there is already oxygen dispersing through the cluster due to the fixed oxygen concentration at the inlet. With zero velocity, yet oxygen present further in the duct, the only possible explanation is through the diffusive transport of oxygen. There is very little difference in the appearance of the oxygen concentration contours for the first quarter, halfway through and three quarters through inhalation plots, Figure 4.7b-d. Although the velocity entering the terminal cluster is greatest in this region, the oxygen concentration at each stage shows little difference. Therefore, the dispersion of oxygen is not related to the airflow and is diffusion dominated. Near the end of inhalation, Figure 4.7e-f, air is still flowing into the cluster, although the velocity is approaching zero in preparation for the direction change. The oxygen concentration

has decreased in the duct as the velocity approaches zero, yet the air entering still contains the inhaled oxygen concentration of 7.279 mol/kg. Therefore oxygen is still diffused into the cluster although the velocity is very small. As soon as the airflow changes direction, Figure 4.7g, oxygen is no longer present to exhale; all oxygen has been absorbed into the alveolar walls. Therefore with no resistance to diffusion at the alveolar walls modelled, the alveolar air properties allow the maximum amount of oxygen to be absorbed by the walls at regular resting respiration.

Another important note from Figure 4.7 is the concentration of the oxygen at the alveolar walls. The alveolar walls never experience the inhaled concentration of oxygen; instead the only oxygen present has been diffused there. Therefore the concentration difference at the walls is just enough to drive diffusion across them. It is clear each alveolus experiences the same concentration differences and no alveolus is able to absorb more oxygen than any other. Therefore, combining these results with the velocity results discussed earlier, each alveolus experiences the same velocities and concentration values, making any sort of averaging required over the terminal alveolar cluster unnecessary. However it is still necessary to determine how the time scale of respiration affects the time scale of oxygen diffusion through the alveolar air. This needs to be considered for the closure of the volume-averaged oxygen transport equation.

4.4.4 Diffusion Dominated Transport

The method of oxygen transport through the alveolar air must be determined. Although the results from Section 4.4.3 show diffusion is the dominant method of transport, this can also be derived theoretically based on the parameters of the system. In order to determine whether the method of oxygen transport in the lungs is advection or diffusion dominated, the Peclet number for the airflow within the terminal cluster can be examined. The Peclet number is the dimensionless number representing the advection transport of a property within the fluid over the diffusive transport of the property within the fluid.

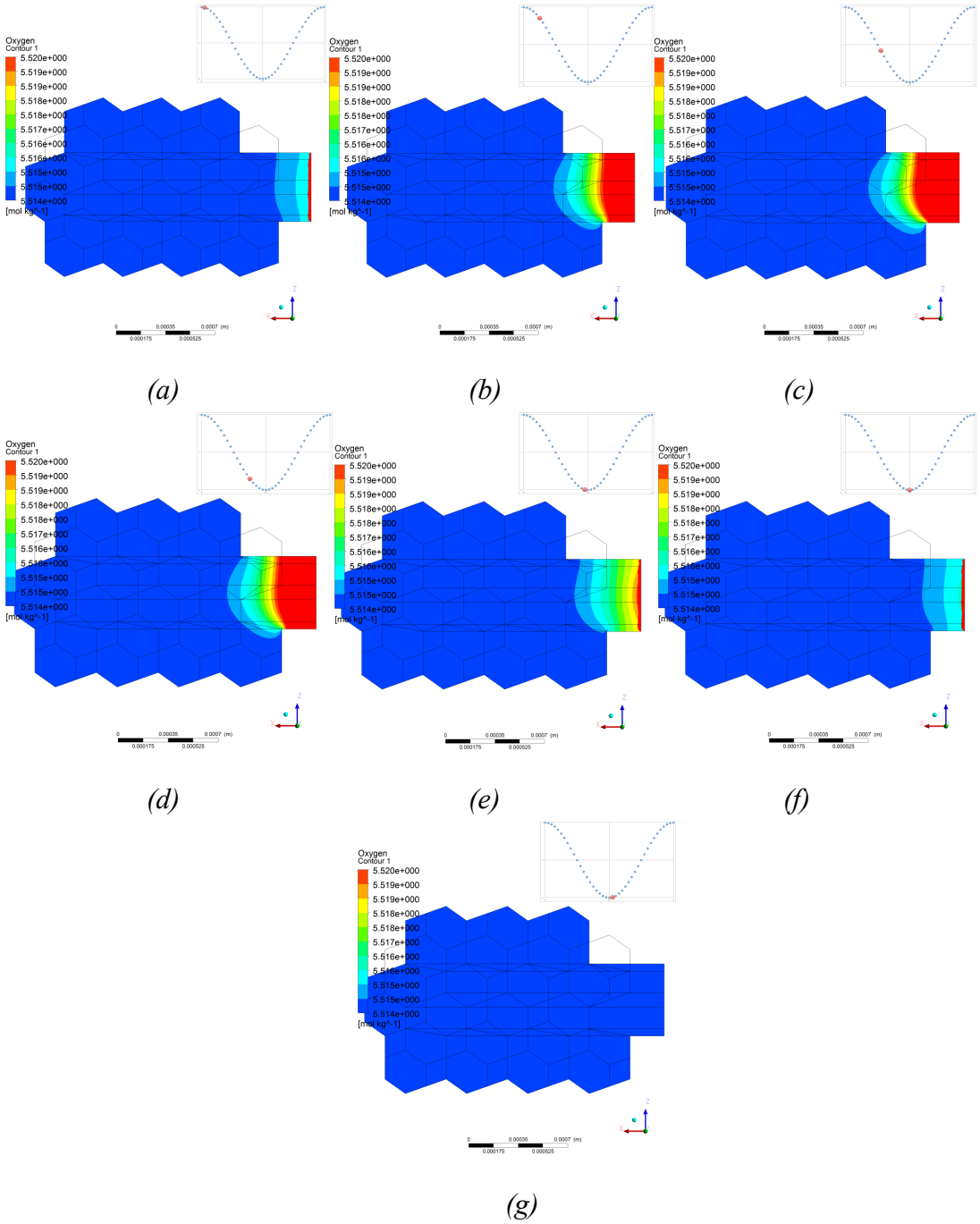

Figure 4.7. *The contour plots for the oxygen concentration in mol/kg are given for the red time point seen in the breathing cycle in the upper right corner of each contour (a) the beginning of inhalation (b) a quarter way into inhalation (c) halfway through inhalation (d) three quarters way through inhalation (e) the second last time step of inhalation (f) the last time step of inhalation (g) the beginning of exhalation. Note the duct has a no flux condition present. These results were for 15% tidal volume expansion with a frequency of one breath every five seconds or 0.2 Hz.*

The Peclet number, *Pe*, is defined as

$$Pe = Re \cdot Sc \tag{4.2}$$

where *Re* is the Reynolds number of the fluid and *Sc* is the Schmidt number of the fluid defined as

$$Re = \frac{\rho u D_H}{\mu} \tag{4.3}$$

and

$$Sc = \frac{\mu}{\rho D_\phi} \tag{4.4}$$

respectively, where ρ is the density of the fluid, μ is the dynamic viscosity of the fluid, u is the velocity of the fluid, D_H is the hydraulic diameter of the pipe and D_ϕ is the diffusivity of species ϕ in the fluid. For Peclet numbers greater than one, transport in the fluid is advection dominated while for Peclet number less than one, the transport is diffusion dominated.

From the velocity results in Section 4.4.2 the maximum Reynolds number of the airflow is approximately 0.04, from the maximum simulated airflow velocity of 1.273×10^{-3} m/s when the hydraulic diameter of the duct was 0.516 mm. For oxygen in ambient air, the Schmidt number is approximately 0.826, yielding a Peclet number of 0.033. This indicates oxygen transport within the alveolar air is diffusion dominated. This is confirmed by the oxygen concentration contours in Figure 4.7, which show the oxygen transport from the inlet to the alveolar walls is a result of diffusion, not advection.

4.4.5 Diffusive Capacity of the Lungs (Simplified Geometry)

Knowing that oxygen is transported through the alveolar air by diffusion, the time scale of oxygen diffusion from the inlet to the alveolar walls needs to be understood in relation to the time scale of respiration. For regular resting respiration, it was determined in Section 4.4.3 the full amount of oxygen entering the terminal cluster can be absorbed based on the properties of the alveolar air. The relation between the two time scales will

be useful in closing the volume-averaged oxygen transport equation and to elucidate how to model the source term in the code. To fully understand the relationship between the time scale of oxygen diffusion and the time scale of respiration, additional simulations were completed on a simplified geometry. The affects of the rate of respiration, tidal volume change and concentration difference between the inhaled air and the alveolar walls on the amount of oxygen able to be diffused through the air can be studied on this simplified geometry. These simulations will help close the volume-averaged species transport equation giving a better perspective on the time scale of oxygen diffusion through the alveolar air.

The geometry used for these additional simulations was a terminal tube with the same length and diameter as the terminal bronchiole modelled in Section 4.1.1. The geometry seen in Figure 4.8 represents the terminal tube used along with the O-grid mesh used to discretize the domain. Although this mesh appears course, required results are qualitative in nature, so the exact value was not relevant. The hydraulic diameter and tube length are equivalent to the terminal alveolated cluster so this tube represents the terminal bronchiole without any alveoli aiding oxygen absorption.

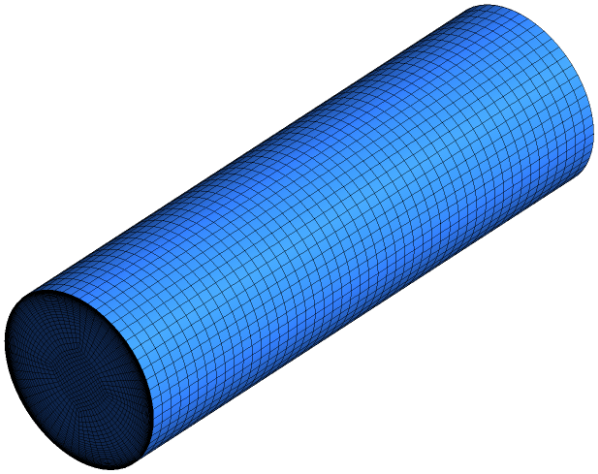

Figure 4.8. *Simplified tube geometry used to determine the difference between the time scale of diffusion and the time scale of respiration based on the alveolar air properties. The coarse O-grid mesh is included for visualization purposes.*

The terminal wall (not seen in Figure 4.8) was assigned a constant oxygen concentration value to represent the alveolar walls, and the cylindrical face was assigned a no flux condition to correspond with no oxygen exchange occurring prior to reaching the alveoli. Therefore oxygen could only be absorbed through the terminal wall. The three different studies completed over a variety of respiration frequencies are described in Table 4.1. The average surface area to volume ratio (SAVR) of the terminal tube was 593.9 m^2/m^3. The maximum amount of oxygen available for absorption by the terminal wall was calculated using the following equation

$$N_{max} = m(c_{inlet} - c_{wall}) \tag{4.5}$$

where N_{max} is the maximum amount of oxygen available for absorption for the given concentration difference in mol, m is the mass of air entering the duct in kg and c_{inlet} and c_{wall} are the oxygen concentrations at the inlet and the wall respectively in moles per kg.

Table 4.1. *The boundary conditions and mesh motion parameters for the three studies run on the terminal tube geometry. Each study contained six different frequencies of respiration.*

Case Number	Tidal Volume	Inlet Oxygen Concentration, mol/kg	Wall Oxygen Concentration, mol/kg	Maximum Amount of Oxygen Absorbed, $\times 10^{-10}$ mol
One	15%	7.279	5.514	0.99529
Two	30%	7.279	5.514	1.9916
Three	15%	16.66	5.514	6.2853

The same mesh motion equations applied to the terminal acinar cluster were applied to the terminal tube, Eqs. 4.1. To calculate the amount of oxygen absorbed into the system, it was necessary to calculate the amount of oxygen entering the inlet and subtract the amount of oxygen being exhaled. Calculating the amount of oxygen absorbed by the terminal wall is not possible in ANSYS® CFX due to the mesh motion.

The amount of oxygen absorbed by the terminal wall per breath was calculated for each case. The results have been plotted in Figure 4.9 for all three cases over six simulated respiration rates. The maximum amount of oxygen available per breath, from Table 4.1 was absorbed for the lower frequencies of respiration in Figure 4.9. Less oxygen was absorbed per breath at increasing frequencies of respiration.

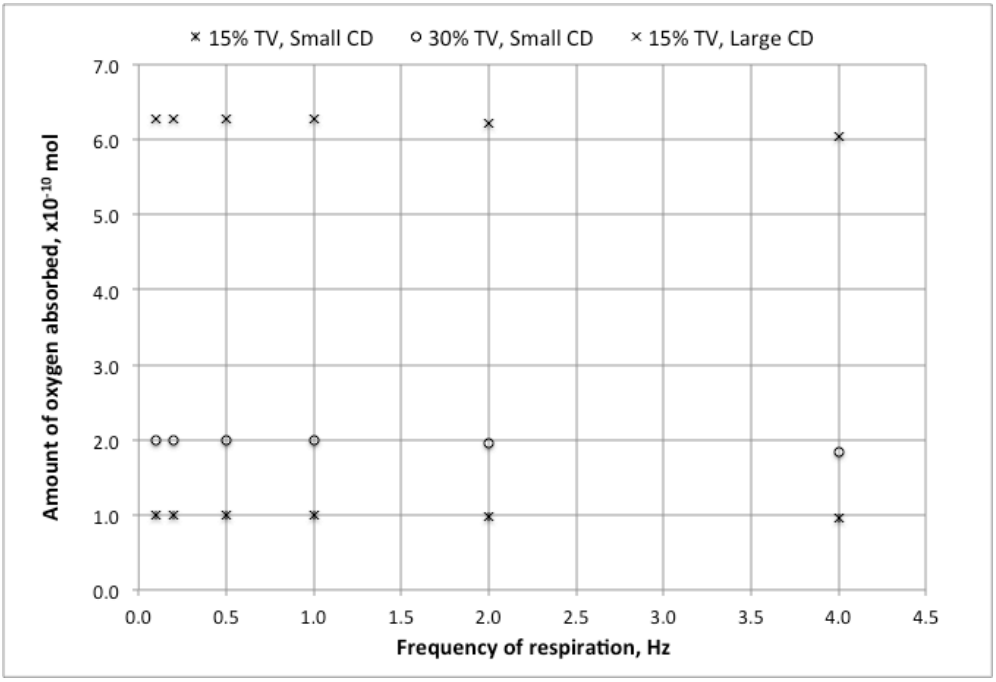

Figure 4.9. *The amount of oxygen absorbed by the terminal tube per breath with respect to the frequency of respiration for all three studies described in Table 4.1. TV = tidal volume, CD = concentration difference between the inlet and the wall.*

The amount of oxygen absorbed per breath has been plotted in Figure 4.10 for the first case with a 15% tidal volume expansion and an atmospheric inlet condition. Figures for the remaining two cases can be found in Appendix A.2. The amount of oxygen absorbed per breath decreases, for the three cases, as the frequency of respiration increases. Therefore the rate of respiration is too fast for the full amount of inhaled oxygen to be absorbed by the far wall, based on the transport properties of the alveolar air, for the larger frequencies.

The SAVR of cases one through three is constant at 593.9 m^2/m^3. Only the terminal wall is able to absorb oxygen due to the no flux condition on the cylindrical wall. However the SAVR for the terminal cluster is 10731 m^2/m^3, giving the terminal alveolar cluster a

SAVR 18× higher than the simplified tube geometry used in the three cases discussed in this section. This difference will have an effect on the total amount of oxygen absorbed per breath across the simulated frequencies. Higher SAVR geometries have more area available for absorption, which has been maximized in the terminal alveolated cluster.

The affect of the SAVR on the total amount of oxygen able to be absorbed per breath was studied by removing the no flux condition on the cylindrical wall of the terminal tube. Instead, a constant oxygen concentration of 5.514 mol/kg was applied. Therefore all walls of the tube were available for absorption. This increased the SAVR from 593.9 m^2/m^3 to 8450.2 m^2/m^3; the terminal cluster is still 1.21× larger. The first case described in Table 4.1 was rerun over the six frequencies of respiration with the new SAVR value. The amount of oxygen absorbed per breath for both cases was plotted in Figure 4.10.

The SAVR appears to have a large effect on the amount of oxygen able to be absorbed per breath. The only difference between the two cases in Figure 4.10 was the SAVR for absorption. The case with the large SAVR maintained the maximum amount of oxygen absorbed per breath regardless of the respiration rate, while the case with the lower SAVR displayed a decrease in the amount of oxygen absorbed per breath for increased respiration rates.

The amounts of oxygen absorbed, over ten seconds of respiration, for the three cases described in Table 4.1 have been plotted in Figure 4.11 with respect to the frequency of respiration. The total amount of oxygen absorbed over the same period appears to be linearly related to the rate of respiration. Therefore, although the total amount of oxygen absorbed per breath decreases at increased respiration rates, the amount of oxygen absorbed over ten seconds increases with respiration rate.

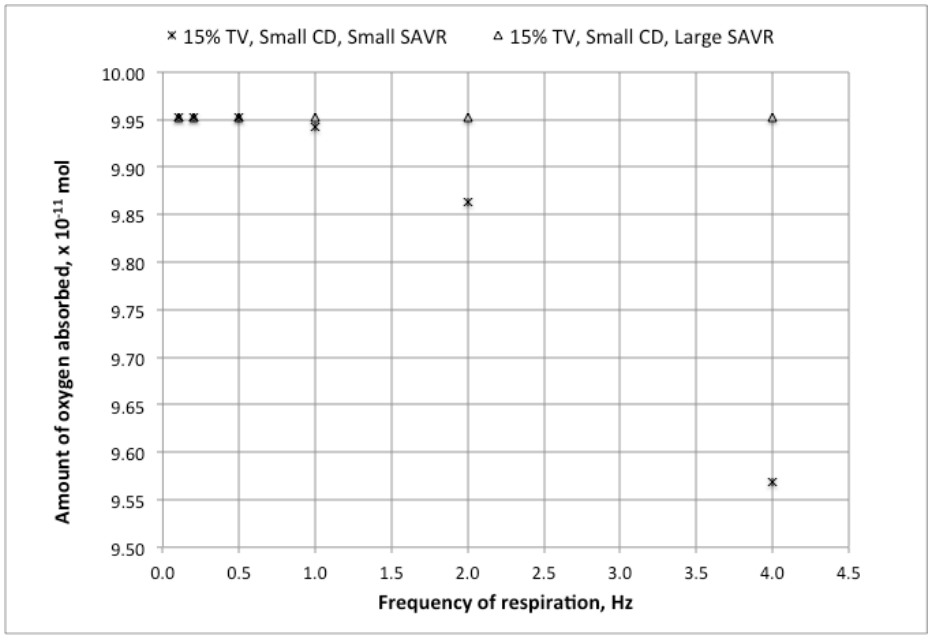

Figure 4.10. *The amount of oxygen absorbed per breath with respect to the frequency of respiration for both large and small SAVR cases. TV = tidal volume, CD = concentration difference between the inlet and the wall, SAVR = Surface area available for diffusion to volume ratio.*

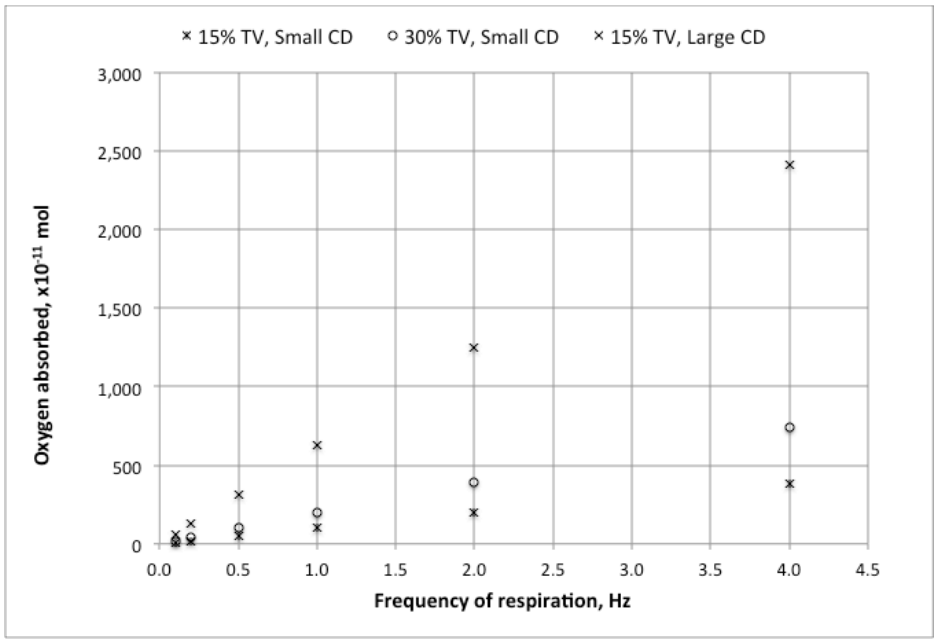

Figure 4.11. *The amount of oxygen absorbed over a ten second period with respect to the frequency of respiration for all three studies described in Table 4.1. TV = tidal volume, CD = concentration difference between the inlet and the wall.*

The three cases plotted in Figure 4.11 displayed a decrease in the amount of oxygen absorbed per breath, yet the amount of oxygen absorbed over ten seconds appears to be linearly proportional to the rate of respiration. With a large SAVR, the maximum amount of oxygen available for absorption is absorbed with each breath over the range of frequencies simulated in this work. Therefore it should follow the same geometry, with a larger SAVR, should absorb more oxygen over the same period for each frequency of respiration. Figure 4.12 plots the amount of oxygen absorbed for both cases plotted in Figure 4.10 over ten seconds of respiration. Although both curves appear to be linear, the slope of the large SAVR curve is greater than the small SAVR curve, as expected.

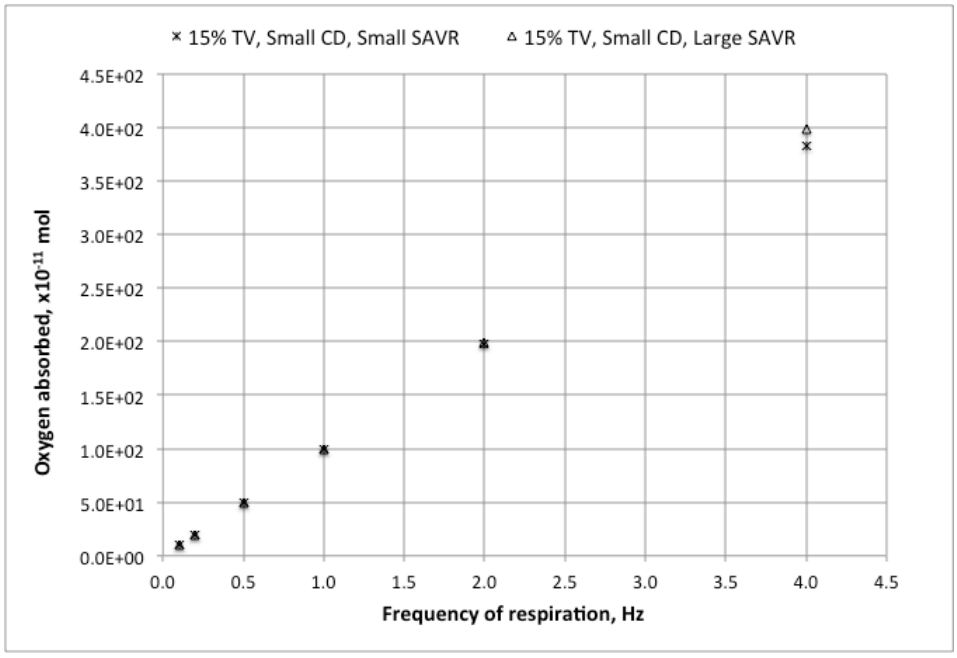

Figure 4.12. *The amount of oxygen absorbed over ten seconds for both large and small SAVR with respect to the frequency of respiration. TV = tidal volume, CD = concentration difference between the inlet and the wall, SAVR = Surface area for diffusion to volume ratio.*

The qualitative results given by the terminal tube simulations elucidate the limitations of the transport properties of the alveolar air. For small SAVR, the time scale of oxygen diffusion through the air is insufficient to allow the full amount of oxygen available to be diffused to the alveolar walls at higher frequencies of respiration. The large SAVR provided enough air for all the available oxygen to be diffused to a transport surface regardless of respiration frequency. These simulations explain the importance of the high

SAVR lung geometry and will help interpret the oxygen concentration results for the terminal acinar cluster, as no previous literature exists for comparison purposes.

4.4.6 Diffusive Capacity of the Lungs (Terminal Alveolar Cluster Geometry)

With no previous literature dealing with concentration equations in a terminal alveolated cluster, terminal tube simulations were completed to determine whether the concentration results for the current simulation were valid. The total amount of oxygen absorbed per breath was plotted in Figure 4.13 for the terminal alveolated cluster with respect to the frequency of respiration. The amount of oxygen absorbed by the lungs per breath is constant within the accuracy of ANSYS® CFX with the differences on the order of 10^{-13} moles.

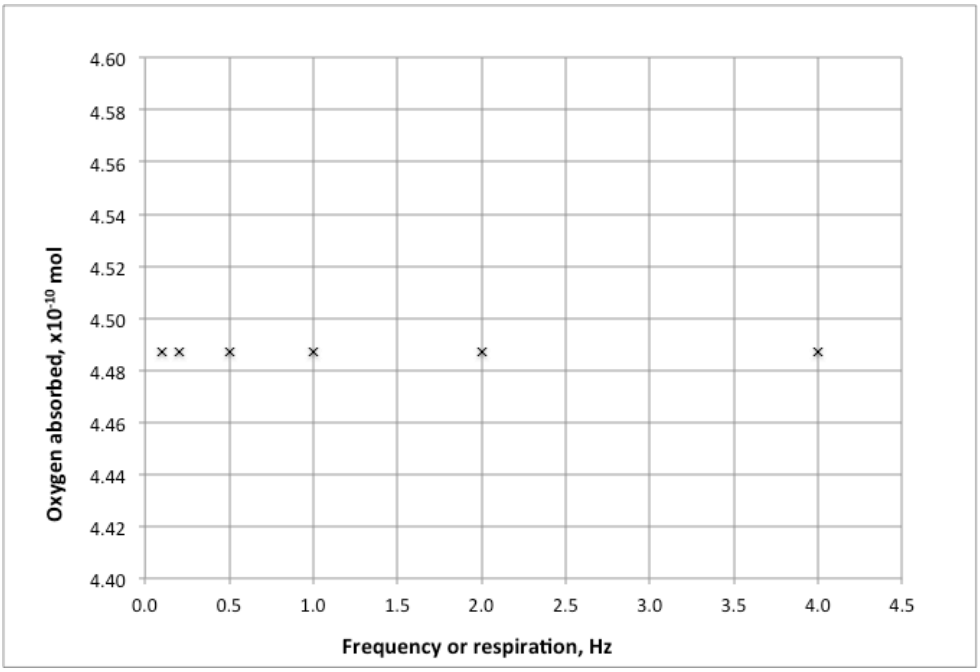

Figure 4.13. *The amount of oxygen absorbed per breath plotted for different rates or respiration. Results are given in terms of 15% tidal volume expansion and the same concentration difference between the inlet and the walls as Figure 4.7.*

In Figure 4.13 the maximum exchange possible between the stated concentrations is 4.4868×10^{-10} moles, calculated using Eq. 4.5 and the change in volume calculated by ANSYS® CFX. Therefore, the amounts of oxygen absorbed for all frequencies seen in Figure 4.13 are equivalent in value, each breath absorbed the maximum amount of

oxygen available. This is consistent with the high SAVR case in Figure 4.10 from the terminal tube simulation. In both cases, the amount of oxygen absorbed per breath is independent of respiration frequency for high SAVR geometries.

Over time the lungs have evolved to have a very large SAVR, making them far more efficient than they need to be under normal respiration conditions. The geometry used for the terminal tube results was equivalent to the terminal bronchiole modelled in the alveolated cluster, without alveoli attached. Therefore, when the small SAVR cases were run, the transport properties of the alveolar air prevented the terminal wall from absorbing all the oxygen present before the oxygen was exhaled at higher frequencies of respiration. However when the SAVR value of the terminal tube was increased, the maximum amount of oxygen was absorbed per breath independent of respiration frequency. There appears to be a critical value of SAVR needed in the lungs for the time scale of diffusion to exceed the time scale of respiration and the larger SAVR terminal tube case appears to be more than sufficient at transporting the available oxygen over the respiration rates simulated in this work.

However the lungs' evolution has increased its SAVR beyond this critical value by introducing alveoli. Therefore the lungs' have a much greater capacity for oxygen transport within the alveolar air than they appear to require. Although at first this capacity seems very high, without a functioning respiratory system, the body will not receive enough oxygen, possibly leading to death within minutes. By increasing the SAVR far beyond what is necessary for survival, the lungs have developed a fail-safe system to ensure the body receives enough oxygen if the lungs are damaged or the air properties change. This allows people to survive with large sections of their lungs removed, or major diseases affecting the lungs with a reasonably good quality of life, as the maximum amount of oxygen can be transported to the alveolar wall.

The amount of oxygen absorbed over ten seconds of respiration was plotted in Figure 4.14 with respect to the rate of respiration. With the same amount of oxygen absorbed per breath, by increasing the frequency of respiration, it follows the total amount of oxygen absorbed over ten seconds is linearly proportional to the rate of respiration and therefore the number of breaths taken in ten seconds.

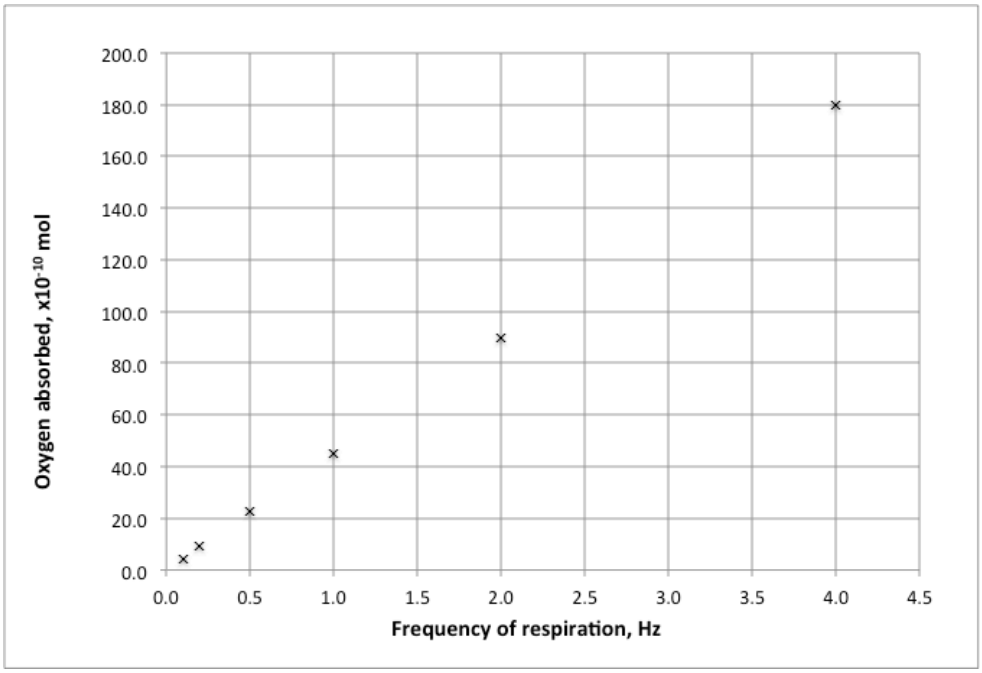

Figure 4.14. *The amount of oxygen absorbed over ten seconds of respiration plotted for different rates of respiration. Results are given in terms of 15% tidal volume expansion and the same concentration difference between the inlet and the walls as Figure 4.7.*

These results show at regular resting respiration rates, all the available oxygen is absorbed into the lungs. Therefore the time scale of oxygen diffusion through the alveolar air far exceeds the time scale of respiration. The amount of oxygen absorbed maintains its maximum potential regardless of respiration frequency. When the frequency of respiration increased beyond realistic rates, the terminal alveolated cluster modelled was still able to absorb the maximum amount of oxygen possible from the air.

These results were maintained in their dimensional form due to the consistent shape and volume of human alveoli [32]. Ochs et al [32] determined the number-weighted mean volume of an alveolus was $(4.2 \pm 0.4)\times10^6\ \mu m^3$. Therefore, the larger the lung volume, the more alveoli present within. Although studying the real geometry of a terminal cluster would have increased the accuracy, this would only apply to one situation. Each terminal cluster will be slightly different; therefore the idealized geometry used in this model could be used.

4.4.7 Time Scale of Diffusion

As the rate of respiration increases, the first three cases of terminal tube results with a small SAVR show the amount of oxygen absorbed per breath decreases. There is not enough time during one breath cycle for the terminal wall to absorb the full amount of oxygen available per breath. This implies the time scale of oxygen diffusion through the alveolar air is not linearly proportional to the rate of respiration; rather it takes the form:

$$t_D \propto \frac{1}{t_R^n} \tag{4.6}$$

where t_D is the time scale of diffusion, t_R is the time scale of respiration and n is a constant.

However the results seen in Figure 4.13 for the terminal acinar cluster do not show any dependency on the time scale of diffusion. The SAVR for the lungs is much higher than the one modelled in the terminal tube as the lungs are composed of approximately 240 million alveoli each, with an average volume of 4.2×10^6 μm^3 per alveolus [32]. To understand how the SAVR affects the amount of oxygen absorbed by the walls, the boundary conditions on the tube were changed so all walls were capable of absorbing oxygen. The terminal tube with the high SAVR showed no dependency on the rate of respiration, Figure 4.10, consistent with the results from the terminal alveolated cluster. Therefore, the effects of the time scale of respiration on the time scale of diffusion are nullified when large SAVRs are present. Therefore for SAVRs larger than a critical value,

$$n = 0 \tag{4.7}$$

thus eliminating the affects of the time scale of respiration on the time scale of diffusion. However for SAVRs below the critical value

$$n \propto (C - SAVR) \tag{4.8}$$

where C is the critical value of SAVR. Therefore SAVR values approaching C would have less affect on the time scale of diffusion than small values of SAVR. For the

purposes of this work, it was unnecessary to determine the critical value of SAVR as the SAVR for the terminal alveolated cluster was above this value.

The dependency on the respiration rate was observed with the terminal tube geometry for different tidal volume expansions, as well as different concentration differences between the inhaled air and the walls. This may explain why from a diffusive air transport approach, during periods of exercise, the respiration rate and the tidal volume of the lungs change. During exercise, the oxygen concentration of the blood returning to the alveoli decreases below the resting level, as the body consumes more oxygen. Therefore the concentration at the alveolar wall drops, creating a larger gradient for diffusion. The body then increases the rate of respiration above resting levels to bring more oxygen into the alveoli, increasing the amount of oxygen available for absorption. The lungs also increase their tidal volume, both increasing the volume of the lungs and the surface area available for diffusion. These three changes (concentration difference, increased rate of respiration and increased tidal volume) ensure the lungs' have the potential to absorb the full amount of oxygen available from the inhaled air, based on the transport properties of the air, at a faster rate than regular resting respiration. Each one of these changes alone would increase the amount of oxygen available for consumption and the lungs perform all three.

The diffusive potential of the lungs is enormous, having been perfected over many years of evolution. Through these pore level simulations, the time scale of the oxygen diffusion through the air is now understood in comparison with the time scale of respiration. Along with this, a better understanding of the method of oxygen transport in the alveolar air has been determined. The motion of oxygen within the terminal bronchioles and alveoli is driven by the diffusion of oxygen through the stale air remaining in the alveoli after the previous respiration. The alveolar walls never experience large oxygen concentration differences, instead only enough oxygen is present within the air at the wall to cause diffusion through the tissue. Therefore for purposes of closing the volume-averaged oxygen transport equation, the absorption of oxygen from the air to the tissue can be modelled by a simple transport term with a low resistance to diffusion.

These simulations did not model the resistance to diffusion within the alveolar walls. By specifying an oxygen concentration at the alveolar walls, the affects of the air properties in controlling the oxygen exchange within the lungs was understood. With a large SAVR the lungs, the maximum amount of oxygen has the potential to be absorbed regardless of respiration frequency. Therefore the air offers no resistance to diffusion in comparison to any resistance offered by the alveolar wall. The affect of the properties of the blood-gas barrier on the amount of oxygen able to be absorbed per breath will be discussed in further detail in Chapter 5.

4.5 SUMMARY OF PORE LEVEL SIMULATIONS

The volume-averaged oxygen transport equation could not be closed without the pore level simulations. By replicating the geometry of a terminal alveolated cluster, the pressure changes, velocities and oxygen concentration changes over a breath cycle could be studied. The small changes in pressure simulated were consistent with the terminal cluster residing at the end of a large airway tree. The pressure decreases as the area and volume increases with each bifurcation. The velocities experienced by an alveolus were very small in comparison to the values experienced in the duct. The position of an alveolus along the duct did not affect the internal alveolar air velocities within. The oxygen concentration contours revealed the transport of oxygen was virtually independent of air motion. Examining the Peclet number of the alveolar air within the cluster confirmed the method of transportation driving the oxygen motion was diffusion, not advection.

The lung tissue was not modelled in these simulations. It was assumed that the tissue could be approximated as having a constant concentration of oxygen. Therefore, these simulations mainly elucidated the relationship between the time scale of oxygen diffusion through the alveolar air and the time scale of respiration. The simplified tube geometry simulations revealed the high SAVR within the alveoli provides the lung tissue with the maximum amount of oxygen available per breath regardless of the respiration rate. The properties of the alveolar air provide no resistance to the transport of oxygen from the

inlet of the terminal cluster to the tissue walls. Therefore, regardless of respiration frequency, the maximum amount of oxygen contained within the inhaled air is available for diffusion into the lung tissue.

Any resistance to oxygen diffusion within the alveoli is a function of the transport properties within the blood gas barrier. Therefore the resistance to diffusion must be appropriately modelled in the closure of the volume-averaged oxygen transport equations for the porous medium using transport properties of the tissue.

CHAPTER 5

CLOSURE MODEL FOR OXYGEN TRANSPORT IN A POROUS DOMAIN

The purpose of this thesis was to develop a framework for oxygen and carbon dioxide exchange in the human lung by using a porous media approach to the lungs' geometry. This chapter covers the closure of the absorption term and the implementation of the volume-averaged oxygen transport equation. The absorption term described in Chapter 3 did not consider the concentration difference between the alveolar air and the alveolar wall. A new absorption term was derived using a volume-averaged form of Fick's law of diffusion giving the exchange an end point. The resistance to alveolar gas diffusion was modelled as a function of tidal volume and the maximum frequency at which the full amount of oxygen available is absorbed per breath. The results included show the simulated species exchange for five frequencies of respiration, proving the viability of the porous media CFD approach to modelling species exchange within the human lung.

5.1 CLOSURE OF THE VOLUME-AVERAGED OXYGEN TRANSPORT EQUATION

Knowing the relationship between the time scale of oxygen diffusion and the time scale of respiration makes it possible to close the volume-averaged oxygen transport equation, Eq. 3.33, by modelling the resistance to oxygen diffusion as a function of tissue properties, as no resistance is offered by the air properties. Closure of the absorption term is necessary to allow the equation to be solved over a porous domain.

5.1.1 Closure of the Absorption Term

The absorption term derived in Chapter 3, Eq. 3.32, is

$$-K_{eq}\frac{A_{fs}}{V}\frac{\partial\langle c_A\rangle^f}{\partial t} \tag{5.1}$$

where K_{eq} is the absorption coefficient, c_A represents the molar concentration of species A per mixture mass in mol/kg, A_{fs} is the interfacial surface area within one control volume in m^2. Whitaker [28] states the absorption coefficient is a function of concentration, c_A, in the event absorption is nonlinear. However this is not relevant to the absorption of oxygen by the lung tissue and for purposes of this work, K_{eq} is constant.

As discussed earlier, the lungs have a large affinity for oxygen absorption, although the oxygen concentration seen at the absorption surface is not much greater than the oxygen concentration of the tissue. Therefore, the absorption of oxygen is fast with a small gradient driving the diffusion at the walls. Whitaker [28] uses an absorption term without including the existence of a concentration of species A at the wall of the solid constituent. Instead, his use of a transient concentration term means as time progresses, the changing concentration changes the amount of oxygen being absorbed. However the work in the previous section reveals the difference between the oxygen concentration of the air at the wall and the tissue's oxygen concentration is very small. During inhalation, the fresh oxygen reaches the inlet of the terminal alveolated cluster and is immediately diffused to the alveolar walls, regardless of the specific location of each alveolus. Therefore, the oxygen concentration experienced by the alveolar walls is either a small gradient, enough to drive diffusion, or the same concentration as the exhaled air. Whitaker's [28] absorption term was not included in this work as no consideration is given to the defined end point of exchange. Whitaker's [28] term implies oxygen concentration will continue to decrease to zero over time, when in actuality the oxygen concentration in the air can only reach the oxygen concentration in the tissue before it is exhaled from the body. Therefore, as the oxygen concentration at the wall affects the amount of oxygen absorbed, it is important to modify Eq. 5.1 to include the concentration difference at the wall.

Another way to determine an appropriate absorption term is by considering absorption as a fundamental process. The amount of oxygen absorbed by the walls can also be determined by taking the flux of the oxygen passing into the tissue and multiplying it by the surface area available for diffusion. Fick's law can be rewritten from the form seen in Eq. 2.1 to

$$J = -D\nabla c_A \tag{5.2}$$

where J is the mass flux of species A in mol·m/kg·s, D is the diffusivity in m^2/s, and ∇c_A is the concentration gradient driving the absorption with the units of mol/kg·m [33]. This flux term can be volume averaged to give

$$-D\langle\nabla c_A\rangle \tag{5.3}$$

which can be expanded using the averaging theorem, Eq. 3.12, to become

$$-D\left[\nabla\langle c_A\rangle + \frac{1}{V}\int_{A_{fs}} \mathbf{n}_{fs} c_A dA\right] \tag{5.4}$$

where the integral term is eliminated with Eq. 3.27 turning Eq. 5.3 into

$$-D\nabla\langle c_A\rangle^i \tag{5.5}$$

The concentration gradient driving the absorption between the air and the tissue, is the difference between the volume-averaged concentration of the fluid and solid constituent multiplied by constant k. Therefore, the volume-averaged flux becomes

$$-k(\langle c_A\rangle^s - \langle c_A\rangle^f) \tag{5.6}$$

where k is the average exchange coefficient with units m/s. The surface area available for absorption per control volume must be multiplied by this volume-averaged flux term to determine the total amount of oxygen absorbed. The resulting absorption term becomes

$$-ka_{fs}(\langle c_A\rangle^s - \langle c_A\rangle^f) \tag{5.7}$$

where a_{fs} is the specific surface area of the porous medium in m^2/m^3. This term provides better numerical control over the transport by having a well-defined end point; when the concentration difference between the solid and fluid constituent becomes zero.

5.1.2 Integration of the Absorption Term

With the help of the pore level simulations described in Chapter 4, it was determined the time scale of oxygen diffusion through the alveolar air was much faster than the time scale of respiration. Replacing Whitaker's [28] absorption term with a volume-averaged version of Fick's law gave

$$-K_{eq}\frac{A_{fs}}{V}\frac{\partial\langle c_A\rangle^f}{\partial t} = -ka_{fs}(\langle c_A\rangle^s - \langle c_A\rangle^f) \tag{5.8}$$

with the resulting volume-averaged species transport equation in the fluid constituent of the porous domain as

$$\varepsilon\frac{\partial\langle c_A\rangle^f}{\partial t} + \nabla(\langle\mathbf{u}\rangle\langle c_A\rangle^f) = D_f\varepsilon\nabla^2\langle c_A\rangle^f - ka_{fs}(\langle c_A\rangle^s - \langle c_A\rangle^f) \tag{5.9}$$

which still required the value of *k*, the average exchange coefficient for the terminal alveolated cluster. As seen in Eq. 5.9, the species transport equation is solved in terms of concentration with the units of kmol per kg not partial pressure.

The volume-averaged concentration equation for the solid constituent becomes

$$(1-\varepsilon)\frac{\partial\langle c_A\rangle^s}{\partial t} = D_s(1-\varepsilon)\nabla^2\langle c_A\rangle^s - ka_{fs}(\langle c_A\rangle^s - \langle c_A\rangle^f) \tag{5.10}$$

by applying the same absorption term from Eq.5.8. Note that *k* is equivalent for both the solid and fluid constituent. These equations are shown in their discretized form in Section 3.7.

The exchange coefficient can be determined using the absorption results from the pore level simulations of the terminal alveolated cluster.

5.1.3 Exchange Coefficient

Examining the velocity and oxygen concentration contour results for the terminal acinar cluster, in Sections 4.4.2 and 4.4.3, reveals each alveolus in the cluster experiences the same conditions. Therefore, each alveolus can be treated equally, without any special averaging required. With the transport of oxygen from the inlet to the wall in the pore level simulations elucidated, the average exchange coefficient for the oxygen diffusion within the lungs can be determined (average in the sense it is derived from results of the entire terminal cluster). The exchange coefficient, k in m/s, is defined as

$$k = \frac{\dot{N}_A}{A\alpha_A\left(c_{A,i} - c_{A,w}\right)} \tag{5.11}$$

where α_A is the solubility of species A in tissue in kg/m^3, A is the average surface area available for exchange during respiration, $c_{A,i}$ and $c_{A,w}$ are the concentrations of species A in mol/kg at the inlet and wall, respectively, and $\dot{N}_A$ is the exchange rate of species A in mol/s. The exchange rate for oxygen in one breath can be calculated by

$$\dot{N}_A = \frac{N_A}{t} = fN_A \tag{5.12}$$

where t is the length of time exchange occurs per breath in seconds, f is the frequency of respiration and N_A can be found in general as:

$$N_A = \sum_{i=1}^{20} \dot{m}_i \Delta t\left(c_{A,inhaled} - \overline{c_{A,exhaled,i}}\right) \tag{5.13}$$

where i is the number of time steps over the exhale, $\dot{m}_i$ is the mass flow rate at each time step in kg/s, Δt is the length of each time step and $\overline{c_{A,exhaled,i}}$ is the mass flow averaged concentration at the outlet in mol/kg. As we are seeking a constant value of k suitable for all calculations, it is useful to consider the maximum amount of oxygen that could be absorbed per breath as supplied by the air:

$$N_{A,max} = \rho \Delta V_T\left(c_{A,i} - c_{A,w}\right) \tag{5.14}$$

where ΔV_T is the tidal volume of the terminal alveolated cluster studied in Chapter 4, ρ is the density of the air mixture. In this manner, Eq. 5.11 combined with Eqs. 5.12 and 5.14 becomes:

$$k = \frac{f\rho\Delta V_T}{A\alpha_A} \tag{5.15}$$

where ΔV_T and A are both parameters from the terminal alveolated cluster, and the frequency f is the only parameter left to be determined.

This coefficient can be recast into a resistance as:

$$R = \frac{1}{ka_{fs}} = \frac{\alpha_A A}{\rho a_{fs}\Delta V_T}\cdot\frac{1}{f} \tag{5.16}$$

where the resistance to diffusion is seen to be inversely proportional to the frequency of respiration. This suggests when the rate of respiration decreases, the resistance to diffusion increases, i.e. one breath every ten seconds will absorb less oxygen per breath than one breath per second, which is not reasonable.

It is more reasonable to expect the exchange coefficient k is constant with respect to respiration frequency, and more dependent on tidal volume. Then, since the model to this point is based on the maximum possible exchange for a given $\Delta\langle c_A\rangle$ and ΔV_T, we propose this frequency should correspond to the maximum frequency where complete exchange can occur.

The time scale for the oxygen diffusion through the blood-gas barrier is

$$\tau \sim \frac{L^2}{D} \tag{5.17}$$

where L is the 2 μm thickness of the barrier and D is the diffusion coefficient of oxygen through tissue at 2.5×10^{-5} cm^2/s [34]. The time scale for diffusion is approximately 0.001667s. Since this is longer than the time scale of diffusion through the alveolar air, the oxygen diffusion should be dependent on the properties of the tissue. Therefore, the

frequency at which the maximum exchange per breath can occur within the lungs for a given tidal volume should be determined based on the properties of the lung tissue.

Rapid breathing, or tachypnea, is defined as a respiration rate greater than 20 breaths per minute, or one breath every three seconds (0.33 Hz). This frequency can also be determined by calculating the time it takes to absorb the full amount of oxygen available per breath. This can be done by multiplying the flux of oxygen into the tissue by the surface area available for exchange, by the solubility of oxygen in the tissue over the thickness of the blood-gas barrier. The maximum amount of oxygen in moles, available for exchange can then be divided by this value. Therefore the minimum time it takes for the full amount of oxygen available per breath to be absorbed by the lungs is

$$t = \frac{N_{max} L}{A \alpha_A D \Delta c_A} \tag{5.18}$$

where N_{max} is the maximum moles available per breath (4.4868×10^{-10} mol from the pore level simulation with a 15% tidal volume), A is the average area available for exchange in the simulated acinar cluster from Chapter 4 (1.662×10^{-5} m^2), D is the diffusivity of oxygen in tissue at 2.4×10^{-9} m^2/s [34], α_A is the solubility of oxygen in tissue at 0.004406 kg/m^3 [35], L is the thickness of the blood-gas barrier at 2 μm, and the change in concentration is the same used in Chapter 4 with the units of mol/kg. Therefore the minimum time to absorb the full amount of oxygen available per breath for a 15% tidal volume is 2.91 s. This makes the maximum frequency at which full absorption is possible, f_m, for a 15% tidal volume approximately 0.34 Hz, the same value mentioned before as rapid breathing.

This maximum frequency can be integrated into Eq. 5.15 giving

$$k = \frac{f_m \rho \Delta V_T}{A \alpha_A} \tag{5.19}$$

This gives the resistance to diffusion in terms of only one changing variable, ΔV_T or tidal volume. As seen in the following equation, the new k term changes Eq. 5.16 to

$$R = \frac{\alpha_A A}{\rho a_{fs}} \cdot \frac{1}{f_m \Delta V_T} \tag{5.20}$$

where f_m is expected to be a function of tidal volume through Eqs. 5.14 and 5.18.

Therefore, as the tidal volume increases, the resistance to diffusion will decrease. This will not only increase the amount of oxygen available for diffusion by drawing more oxygen into the alveoli, but it will also increase the surface area available for exchange. The values of A, α_A, a_{fs}, and ρ are constants and are either parameters of the tissue or air. The only two parameters with control over the resistance to diffusion are the tidal volume of the terminal alveolated cluster and the maximum frequency at which all the oxygen can be absorbed per breath.

5.2 SIMPLIFIED COMPUTATIONAL MODEL

Due to the complex geometry and function of the lungs, it is necessary to make various assumptions and simplifications in order to comply with current modelling techniques [1,13-17,19-21,25-27]. The approach used for the present model required assumptions to simplify the problem within the scope of this work. These assumptions are listed within this section.

5.2.1 Geometry

Modelling the entire lung was not required to develop the framework for oxygen and carbon dioxide exchange within a porous medium; therefore a smaller domain was used. The domain size was arbitrarily set to 6.0 cm × 4.0 cm × 2.0 cm. With more than three quarters of the lungs' air volume residing within the 20th to 23rd generations [18], this was assumed to be a reasonable size for a section of terminal alveoli.

The structured orthogonal grid used to discretize the porous domain did not allow mesh expansion therefore no domain changes during respiration were possible. To maintain the conservation of mass equation without expansion, a separate inlet and outlet were used instead of the shared inlet/outlet of a regular expanding lung [26]. Therefore, fresh

air would be moved through the porous domain to simulate respiration with flow velocities in one direction. Uniform properties of porosity, permeability and density were maintained throughout the domain.

5.2.2 Respiration Cycle

Although evidence exists claiming inhalation and exhalation have different airflow velocities [21], respiration was assumed to be sinusoidal. Five different rates of respiration were tested including regular resting respiration of 12 breaths per minute for an adult, placing this work within the range of multiple previous studies [9,19,25,26].

5.2.3 Species Exchange between the Fluid and Solid Constituents

The bifurcating geometry of the lungs' airway tree means the air velocities at the alveolar level are very small. With species exchange limited to the alveolar walls (not occurring within the bronchioles) [5,9,18], exchange occurs only when small air velocities are present. Without an expanding domain, modelling small, inhaled velocities changing direction was not feasible. Instead it was assumed exchange would only occur when the sinusoidal through flow velocity was near zero, to simulate fresh air reaching the terminal alveoli before any exchange occurs. This approach would exhale the oxygen-depleted air between breaths, allowing fresh air to replace it.

Before the exchange coefficient k could be calculated, the amount of time exchange was permitted in the porous medium needed to be determined. The total amount of oxygen, in moles, absorbed per breath could be extracted from the pore level simulations from Chapter 4. However, this value was allowed to exchange over the full length of the respiration in those simulations. Although this occurs naturally in the lung, the simulated lung tissue used in this work required a through flow of oxygen. If exchange were permitted throughout each respiration, the results would show little variation during the respiration cycle and the tissue farthest from the inlet would never be exposed to any oxygen. Therefore, the exchange between the air and the tissue would be permitted when the velocity of the airflow was 0.005 m/s or less, or one fifth of the respiration cycle corresponding to the lowest airflow velocities as seen in Figure 5.1.

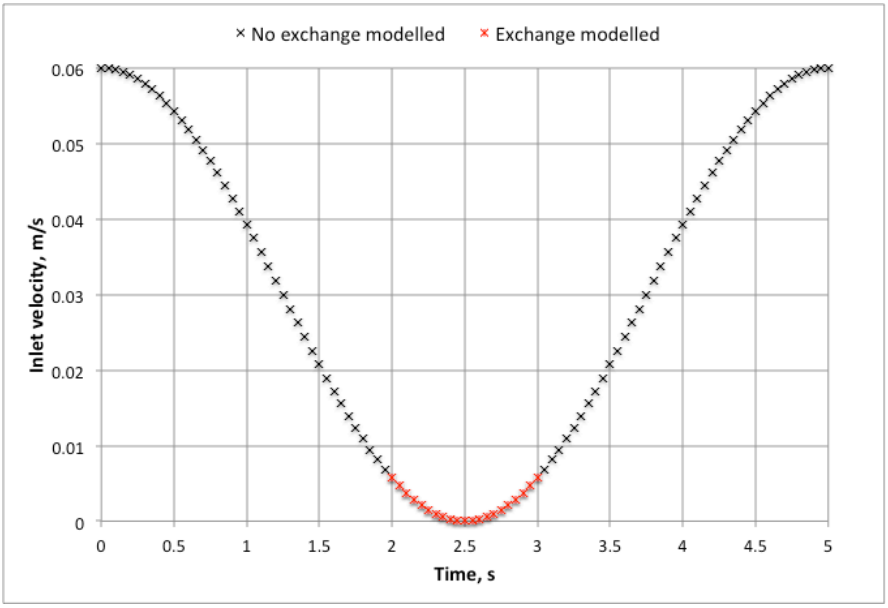

Figure 5.1. *The periodic inlet velocity condition for a regular resting breath cycle of one breath very five seconds. The time steps were oxygen exchange was calculated between the air and the tissue are shown in red.*

With oxygen exchange limited to one fifth of the total breath cycle, the length of time exchange can occur, t in Eq. 5.12, would be dependent on the frequency of respiration. Therefore the exchange coefficient, k, becomes

$$k = \frac{5 f_m \rho \Delta V_T}{A \alpha_A} \tag{5.22}$$

and the resistance to diffusion modelled by the system becomes

$$R = \frac{\alpha_A A}{5 \rho a_{fs}} \cdot \frac{1}{f_m \Delta V_T} \tag{5.23}$$

with the necessary restriction to the oxygen exchange in the porous domain included.

The value of k required for the closure of the absorption term in the volume-averaged oxygen transport equation in the porous media is 5.904×10^{-3} m/s for the simulated 15% tidal expansion. This value of the exchange coefficient will allow the maximum amount of oxygen to be absorbed for respiration rates lower than the maximum frequency, f_m, as sufficient time between breaths is available for the full absorption. However, if the frequency of respiration is greater than the maximum frequency, the time scale of

respiration exceeds the time scale of diffusion and the full amount of oxygen can not be absorbed before exhalation.

5.2.4 Modelling the Lung Tissue

Another consideration when modelling the lung tissue is the existence of blood within the capillaries on the other side of the blood-gas barrier. Introducing a removal mechanism was beyond the scope of this work; therefore the removal of oxygenated blood by the capillaries was modelled by increasing the diffusivity of the solid constituent. All oxygen absorbed by the solid constituent would be immediately transported through the boundaries. The boundary conditions applied are discussed in detail in Section 5.3.

5.3 BOUNDARY AND INITIAL CONDITIONS

The boundary conditions applied in this model were imposed so the simulation would represent the conditions in the alveoli as accurately as possible. Described here are the boundary and initial conditions applied to the porous domain. Two types of boundary conditions were used in this work, Dirichlet and Neumann conditions.

5.3.1 Velocity

The velocity at the inlet of the porous domain was specified using a transient boundary condition to simulate respiration. Without an expanding mesh, it was necessary to force fresh air though the porous domain to model respiration. As seen in the pore level simulations, the maximum magnitudes of velocity present within the terminal cluster were approximately 0.0013 m/s in the duct while the velocities seen by the alveoli were much smaller. In order to fully exhale the depleted air from the porous domain, the maximum velocity simulated was 0.060 m/s due to the length of the model. Although this is faster than the simulated velocities mentioned earlier, the exchange between the two constituents was only allowed when the velocity of the air was 0.005 m/s or less. The inlet velocity was defined as

$$u_{inlet} = A\cos(\omega t + \phi) \tag{5.24}$$

where A is the amplitude of the velocity at 0.03 m, ω is the frequency of respiration, t is the time and ϕ is the phase shift of 0.03 m preventing negative velocities. The inlet velocities in the y and z directions were set to zero using a Dirichlet condition. The velocities were initialized to zero in the y and z directions and 0.06 m/s in the x direction.

The velocity at the outlet was defined with a Neumann condition specifying no change in the derivative of velocity across the border for all three directional components of velocity. At the remaining boundaries, no slip conditions were applied.

5.3.2 Pressure

The pressure at the outlet was set to zero using a Dirichlet boundary condition. The pressures at all remaining walls, including the inlet, were extrapolated from the previous cell. The pressure throughout the domain was initialized to zero.

5.3.3 Oxygen Concentration

The boundary conditions for oxygen concentration were different for both the fluid and solid constituent; in the same manner the conditions in the lungs are different for both the air and the tissue. As mentioned in Section 5.2.4, to account for the continual removal of oxygenated blood from the lungs, the solid constituent was modelled with a large oxygen diffusivity. A Dirichlet boundary condition was applied to all walls of the domain except the outlet. This condition set the oxygen concentration at the boundaries to the same value air exits the lungs with. When respiration occurs, the difference in concentration across the blood-gas barrier causes oxygen to diffuse through the barrier, equalizing the concentration on either side. However the blood is in constant motion, moving the increasingly oxygenated blood along the capillaries. This results in the alveolar walls seeing a constantly low value of oxygen concentration. As exchange occurs between the air and the tissue, the concentration of the air decreases until matching the concentration of the tissue before being exhaled. A Neumann condition was used at the outlet wall so no flux was present between the cell preceding the outlet and the outlet itself.

The concentration of oxygen in the fluid constituent, the air, was more complicated. At the inlet, a Dirichlet condition was used to set the inhaled, fresh air to the atmospheric concentration of oxygen in kmol/kg. The outlet was set using a Neumann condition to extrapolate the value of the concentration at the outlet from the concentration in the preceding cell. The remaining four walls were specified using Neumann symmetry conditions, simulating the continual nature of the alveolar region beyond the imposed domain of this model.

The concentration of the oxygen in the solid constituent was initialized to have the same value as the boundaries; the oxygen concentration in exhaled air. The fluid constituent was initialized to the same concentration at which oxygen is inhaled to allow the simulation to commence at the beginning of inhalation.

5.4 SPATIAL AND TEMPORAL INDEPENDENCE

The results must be both spatially and temporally independent, therefore the mole fraction of exhaled oxygen was measured for four simulations with two different grid sizes and two different time step lengths. The two grid sizes were 8,000 and 64,000 orthogonal volumes, with one breath cycle occurring over 50 and 100 time steps. Doubling the number of control volumes in the x, y, and z direction created the larger grid size. The percent difference between the small mesh with 50 time steps (Δt = 0.1s) and the large mesh with 100 time steps (Δt = 0.05s) was 0.00951% for a respiration rate of one breath every five seconds. Therefore, the larger grid size with 100 time steps was used for the remainder of this work. This mesh is represented in Figure 5.2.

Due to the number of control volumes dividing up such a small domain, it was important to check the average size of an alveolus compared to the size of each control volume. The volume contained with each control volume is 7.5×10^{9} μm^3 while the average volume of an alveolus is 4.2×10^{6} μm^3 [32]. With a porosity of 0.9 [18] the approximate number of alveoli present in one control volume is 1610. Therefore this mesh size was appropriate for these simulations.

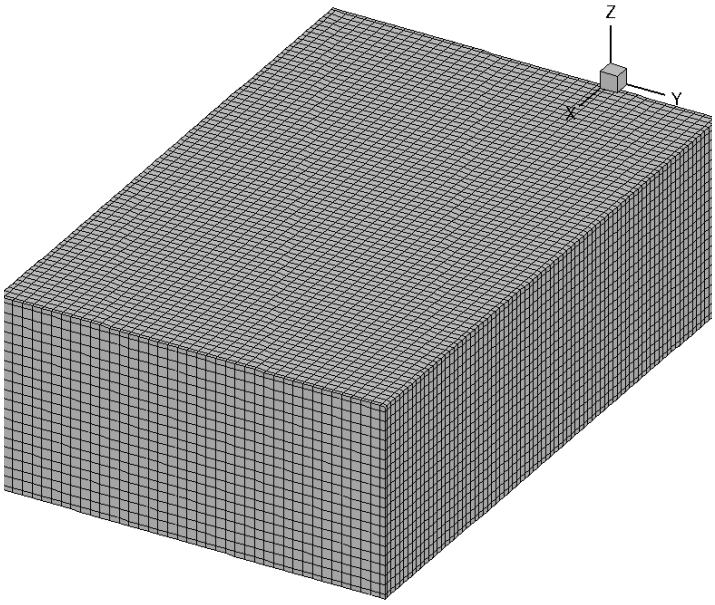

Figure 5.2. *The large mesh used to produce the remainder of the results discussed in this chapter with 64,000 control volumes.*

5.5 RESULTS

The proposed model is unique among lung models by using a porous media volume-averaged approach to calculate the concentration of oxygen and carbon dioxide within the lungs. Therefore it is important to compare the results from these simulations with the expected exhaled values of both oxygen and carbon dioxide. Due to the periodic inlet velocity, the results must be time-periodic are no differences in the calculated concentration of the gases after multiple respirations are noted.

The velocity and pressure results were not included here as the mass and momentum equations have already been verified by Betchen et al [8] and the porous plug test case can be found in Appendix A.1. Therefore, the focus of this chapter will remain on the implementation of the mass transfer equation for the oxygen exchange and the separate carbon dioxide exchange calculation.

5.5.1 Oxygen Concentration Contours in the Fluid

With the volume-averaged oxygen transport equation implemented, the contour plots of the oxygen concentration for each time step could be plotted. The contour plots for selected time steps have been plotted in Figure 5.3 for a regular resting respiration rate of one breath every five seconds, the same frequency the oxygen concentration contours were plotted with in Chapter 4. The inlet lies on the left side of the contour plots in Figure 5.3 and the outlet lies on the right.

The oxygen concentration in the air was held constant until the velocity was 0.005 m/s or less, then exchange was allowed to occur. Therefore in Figure 5.3a the concentration is constant with the inhaled atmospheric composition of 21% oxygen. Oxygen exchange is occurring in Figures 5.3b-e and the contour plots show the oxygen concentration at the outlet is dropping. A common feature of the four plots, is oxygen concentration near the inlet being much greater than the concentration near the outlet. This is a result of the lack of mesh motion and the requirement to have a through flow instead of a reversing flow, like the flow seen in the previous chapter. Although exchange occurs when the inlet velocity is very slow (refer to Figure 5.1) atmospheric air is still entering the porous domain while the exchange is occurring. Therefore, as oxygen is depleted from the air during exchange, on the left side of the domain more oxygen is continually being introduced.

Once exchange ceases, the air with the low oxygen concentration is forced out of the domain by incoming atmospheric air. This can be seen in Figures 5.3f-l. The incoming air does not replace the depleted air; instead the incoming air mixes with the old air, slowly raising the total oxygen concentration until the entire domain is again filled with atmospheric air.

At the end of one breath cycle for the simulation represented in Figure 5.3, the air within the porous domain has been fully replaced once again by atmospheric air. Therefore, the next respiration has the same starting condition as the preceding one.

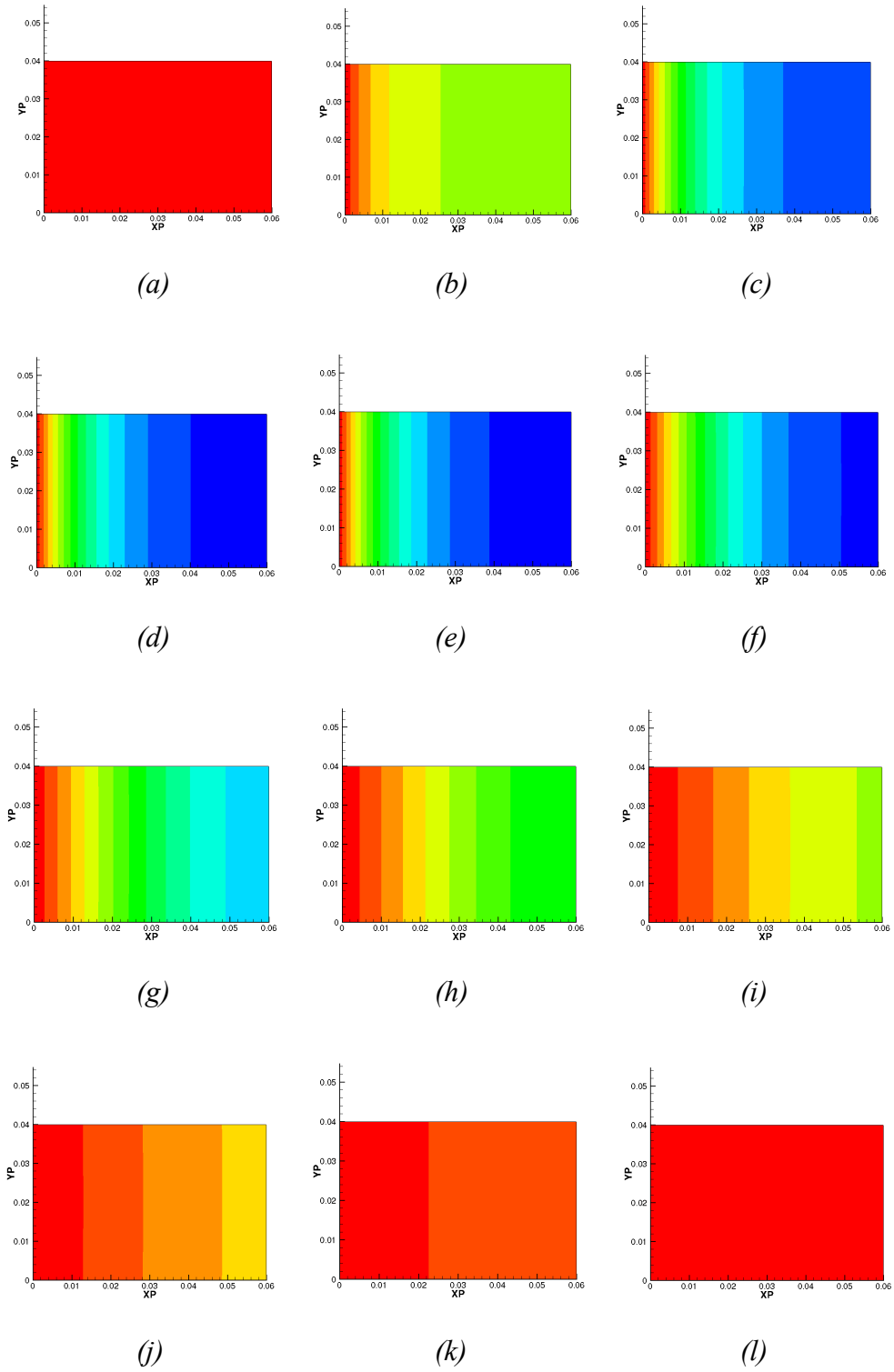

Figure 5.3. *Concentration of oxygen contours, (a) last step of inhalation before exchange occurs, (b)-(e) various steps while exhale occurs, (f)-(l) exchange no longer occurs and high concentration air is replacing and mixing with low concentration air before being pushed out. Red = high oxygen concentrations, Blue = low oxygen concentration.*

The contours represented in Figure 5.3 are all vertical, corresponding to the effects of plug flow on the oxygen concentration distribution. The effect of the porous structure on the fluid is similar to applying a very large viscosity to an unhindered fluid.

5.5.2 Time-Periodic Transport Results

Ten breath cycles were simulated for five frequencies of respiration tested with the model; 0.1 Hz, 0.2 Hz, 0.34 Hz, 0.5 Hz, and 1.0 Hz. This ensured any affects of the initial condition were washed out and the results were time-periodic. The largest percent difference of the exhaled oxygen compositions between the first and last breath was 0.4% at the fastest rate of respiration (1.0 Hz). Therefore the following results were considered to be time-periodic.

The amount of oxygen and carbon dioxide exhaled for each frequency has been plotted in Figure 5.4. For the two frequencies tested below the maximum frequency of 0.34 Hz, and the maximum frequency for the 15% tidal volume expansion, the exhaled compositions of air is approximately 17.1% oxygen and 3.9% carbon dioxide, as expected.

The amount of carbon dioxide exhaled for the three lowest frequencies of respiration, which display the maximum possible exchange with each breath, is slightly under the expected value of 4%. Therefore the model appears to be extrapolating the correct value of carbon dioxide exchange from the calculated oxygen composition value. This is consistent with the crude approximation used to determine the amount of carbon dioxide exhaled; therefore the remainder of this discussion will focus on oxygen transport.

The amount of oxygen absorbed per breath by the porous medium decreases as the respiration frequency increases beyond the maximum frequency of 0.34 Hz. This is confirmed in Figure 5.5, which plots the total amount of oxygen absorbed per breath with respect to the frequency of respiration. This plot displays how the amount of oxygen absorbed per breath decreases once the maximum frequency for the current tidal volume is reached, consistent with the expected results described in Section 5.2.3.

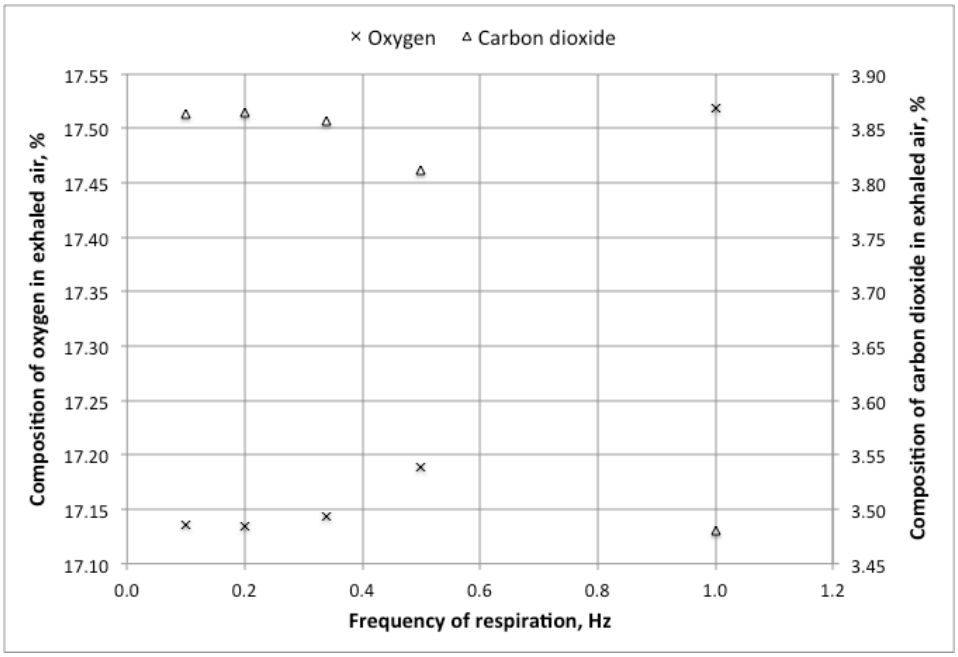

Figure 5.4. *The exhaled percent compositions of both oxygen and carbon dioxide for the tenth breath plotted with respect to the rate of respiration.*

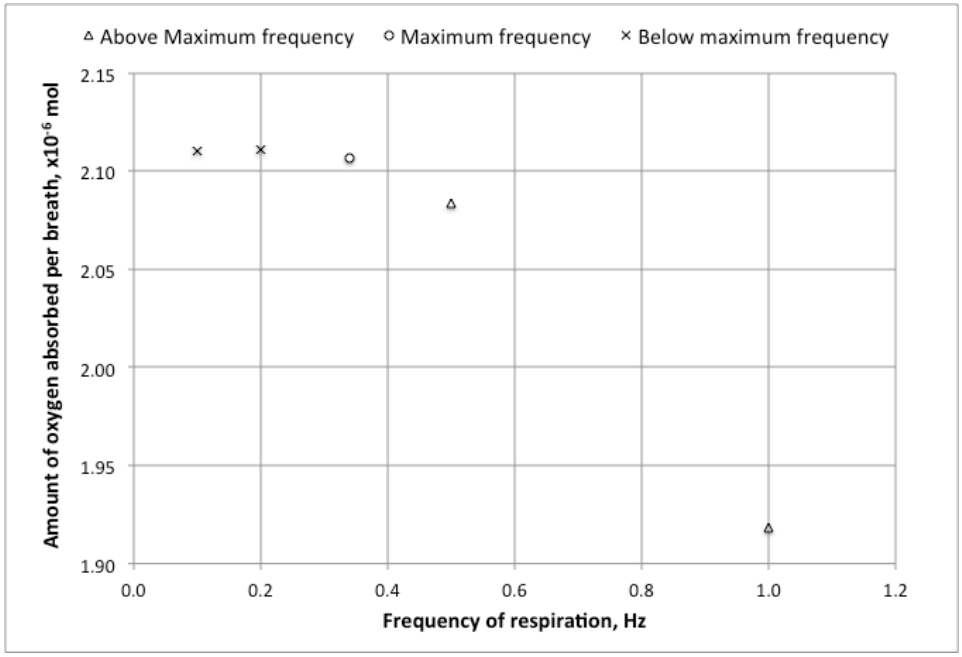

Figure 5.5. *The amount of oxygen absorbed per breath with respect to the rate of respiration, the plot is divided into respiration frequencies above and below the maximum frequency of respiration for which all the available oxygen is absorbed for a 15% tidal volume expansion.*

The resistance to diffusion is modelled as a function of tidal volume with Eq. 5.23. The maximum frequency at which the full amount of oxygen available for the given tidal volume can be absorbed is 0.34 Hz for the 15% tidal volume expansion simulated in this series. Therefore, for frequencies of respiration greater than the maximum frequency, the time scale of diffusion is greater than the time scale of respiration resulting in oxygen being exhaled before the tissue could absorb the full amount available. Less oxygen is able to be absorbed per breath as the frequency of respiration increases, as seen in Figure 5.5. The time scale of diffusion is equivalent to the time scale of respiration for the maximum frequency. As seen in Figure 5.5, the length of time per breath for which exchange was allowed, for the maximum frequency of respiration and the two slower rates modelled, was sufficient to absorb the full amount of oxygen per breath cycle.

The amount of oxygen absorbed by the tissue during ten seconds of respiration has been plotted in Figure 5.6. The maximum frequency, like the two slower frequencies, was able to absorb the full amount of oxygen available every breath cycle. Therefore, by increasing the number of breath cycles, the total amount of oxygen absorbed will increase linearly until the maximum frequency of respiration is reached, as seen in Figure 5.6. The two frequencies of respiration simulated, faster than the time scale of diffusion, were unable to absorb the full amount of oxygen available per breath. However by increasing rate of respiration, these frequencies were able to absorb more oxygen in the 10 second time period since there were more breath cycles. Therefore, although the efficiency per breath cycle is decreased, over the same time period, the tissue absorbed more oxygen due to the increased number of breath cycles occurring. The amount of oxygen absorbed over ten seconds is no longer linear once the time scale of respiration exceeds the time scale of diffusion and the maximum amount of oxygen absorbed is no longer linear.

The resistance to diffusion within the tissue is modelled with a constant value depending on the amount of oxygen available in each breath, the transport properties within the tissue and the length of time the full amount of oxygen available can be absorbed. By simulating various frequencies of respiration, the only changing parameter between the simulations was the length of time oxygen was exposed to the tissue for diffusion purposes. The amount of oxygen absorbed per breath for the simulated frequencies was

dependent upon the time scale of diffusion compared to the time scale of respiration. Therefore each tidal volume expansion will have a different maximum frequency based on the length of time the full amount of oxygen available can be absorbed by the tissue.

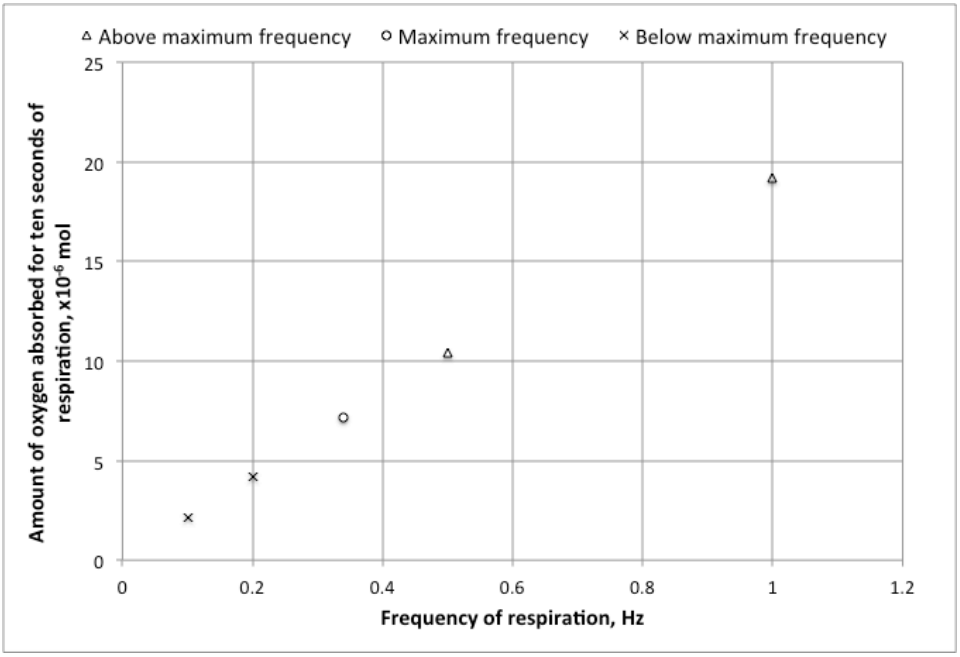

Figure 5.6. *The amount of oxygen absorbed over ten seconds of respiration plotted with respect to the frequency of respiration. The plot is divided into respiration frequencies above and below the maximum frequency of respiration for which all the available oxygen is absorbed for a 15% tidal volume expansion.*

With one tidal volume expansion simulated in the present series of results, one maximum frequency was tested. The effects of the time scale of respiration on the amount of oxygen absorbed by the tissue were examined in this work due to the constant time scale of diffusion lying within the respiration frequencies simulated.

Although it is possible to use this model to test a range of tidal volumes, only one was simulated for this work. The simulated 15% tidal volume expansion was chosen to correspond with a tidal volume of 500 ml for a 4.5 L lung capacity during regular resting respiration with approximately 80-90% of the volume stored in the alveoli [18]. The tissue parameters used to calculate the exchange coefficient were assumed to be valid for regular resting respiration. Therefore, the properties used may require revision for

different tidal expansions, limiting the results shown in this work to the resting tidal volume simulated. This will be discussed further in Section 6.3.

5.6 MODEL VIABILITY

The model developed and tested in this work simulates the expected results for exhaled oxygen and carbon dioxide composition values. For the tested tidal volume, the model responded accordingly to the effects of the rate of respiration on the amount of oxygen absorbed. With the method for determining the overall resistance to diffusion, discussed in Section 5.2.3, it is possible to determine the value of the exchange coefficient, k, for different tidal volumes or concentration differences. This model is viable due to its resistance to oxygen diffusion given in terms of the tissue parameters, Eq. 5.23. If the required parameters change, the simulated resistance will respond accordingly in the expected way observed within the lungs. The volume-averaged oxygen transport equation introduced in this work included the properties of both the air and the tissue in controlling the amount of oxygen able to diffuse into the lungs for a given breath.

5.7 SUMMARY

The model developed in this work was able to use a volume-averaged oxygen transport equation to solve for the oxygen concentration in alveolar air during respiration. The pore level simulations discussed in Chapter 4 revealed that the limitation to oxygen transport was a result of the resistance in the tissue. If the resistance to diffusion through the tissue were not simulated, the transport of oxygen through the alveolar air would be sufficient to achieve the maximum available absorption with every breath regardless of respiration rate. However, the resistance to diffusion simulated by the porous medium model included the effects of the tissue properties in limiting the amount of oxygen exchanged per breath. Therefore, the time scale of alveolar oxygen diffusion is dependent upon the diffusion rate of the tissue not the properties of the alveolar air.

The volume-averaged concentration equation was implemented into the code described by Betchen et al [8] and the oxygen concentration in the air was calculated over 100 time steps per breath for ten breath cycles across five rates of respiration. The maximum frequency for the studied tidal volume and the two slower frequencies allowed sufficient time for the full amount of oxygen available to diffuse into the tissue. However, once the rate of respiration was faster than the time scale of diffusion, oxygen was exhaled before the full amount could be absorbed. Therefore, it can be concluded this model provides a viable new method for calculating the exchange of both oxygen and carbon dioxide within the alveolar region of the lungs.

CHAPTER 6

SUMMARY

6.1 CONCLUSIONS

The porous media CFD model introduced in this thesis proves to be a viable new alveolar exchange model. The volume averaged oxygen transport equations were closed using a volume-averaged form of Fick's law of diffusion giving the oxygen exchange between the alveolar air and the tissue an end point once the concentrations of each constituent are equivalent. The closure of these equations was conditional upon understanding the relationship between the time scale of oxygen diffusion in the alveoli and the time scale of respiration. Pore level simulations were completed, using a terminal acinar cluster containing 22 alveoli, to elucidate this relationship. The resistance to the transport of oxygen into the tissue was not modelled during these simulations so the time scale of oxygen transport through the alveolar air could be studied.

The pore level simulations revealed each alveolus experiences the same airflow velocities and concentration differences regardless of its location in the terminal cluster. The pressure and airflow results simulated were consistent with the location of a terminal cluster and previous studies with similar idealized geometry [19-21]. With no literature examining oxygen concentration at this level, additional simulations were completed using a simplified tube geometry to compare the effects of the alveolar air's oxygen transport properties on the time scale of diffusion, when different conditions were simulated. These pore level simulations determined the alveolar air is able to provide the tissue surface with the maximum amount of oxygen inhaled for each breath. The alveoli's large surface area available for diffusion to volume ratio ensures this is possible for any rate of respiration. Therefore the resistance to pulmonary oxygen diffusion is a product of the tissue transport properties. From this understanding, the variables used to calculate the exchange coefficient required for the closure of the volume-averaged oxygen transport equations, were properties of the tissue, not the alveolar air.

Due to the requirement of through flow in the porous medium simulated for this thesis, exchange was modelled during one fifth of the respiration cycle, when the velocity of the airflow was 0.005 m/s or less. This was implemented to simulate the small airflow in the terminal alveoli as exchange occurs. The exchange coefficient was altered to accommodate oxygen exchange for one fifth of the entire breath cycle. However this introduced a dependency on the frequency of respiration into the modelling of the resistance to diffusion. The maximum frequency at which the entire amount of oxygen available can be absorbed per breath was used in this resistance term to eliminate the dependency on respiration frequency. Therefore, the resistance to oxygen diffusion within the lung tissue is dependent upon the time it takes to absorb the full amount of oxygen available. This term is a function of tidal volume, as the greater the tidal volume, the more oxygen drawn into the lungs per breath and the more surface area available for oxygen exchange.

The porous medium model was tested for five different frequencies of respiration with one tidal volume to determine the viability of the model. When the time scale of oxygen diffusion was equivalent or less than the time scale of respiration, the maximum amount of oxygen was exchanged between the alveolar air and the tissue. These respiration frequencies exhaled the expected oxygen and carbon dioxide components. However, when the time scale of diffusion was greater than the time scale of respiration, oxygen was exhaled from the porous domain before the full exchange was able to take place. Therefore, respiration was more efficient for slower rates of respiration.

The amount of oxygen absorbed by the lung tissue for ten seconds of respiration was examined. For the three lowest respiration rates tested, each able to absorb the maximum amount of oxygen available per breath, the amount of oxygen absorbed over ten seconds of respiration increased linearly as a function of respiration rate. However, the rates of respiration tested which were greater than the maximum frequency, although not as efficient for each breath cycle, were able to absorb the most amount of oxygen over the ten seconds due to the increased numbers of respirations.

This model provides a viable alternative to previous alveolar models by combining the affects of both the air and tissue properties in controlling oxygen transport within the

human lungs. This model integrates airflow simulations with species concentration in a porous domain and has developed a framework for alveolar gas exchange for both oxygen and carbon dioxide.

6.2 CONTRIBUTIONS

The contributions of this thesis have been summarized here:

- A closure model was developed for the volume-averaged oxygen transport equations in a porous domain based on properties of the alveolar air and lung tissue. A volume-averaged form of Fick's law of diffusion is used to represent the oxygen exchange between the fluid and solid constituents. Pore level simulations on an idealized terminal alveolated cluster were used to determine the appropriate method for simulating the resistance to alveolar gas diffusion by elucidating the relationship between the time scale of respiration and the time scale of oxygen diffusion.
- A framework for modelling oxygen and carbon dioxide exchange in a porous medium has been developed and implemented into an existing 3D conjugate code developed by Betchen et al [8]. This model has the capability to calculate the concentration of oxygen within both the fluid and solid constituent and extract the amount of carbon dioxide exchanged once oxygen exchange has occurred. The parameters of this model can be changed to simulate different conditions present within the lung.

6.3 RECOMMENDATIONS FOR FUTURE WORK

The viability of this model can continue to be explored using different tidal volumes and concentration differences. The effects of these differences can be examined over various frequencies, including the maximum frequency for each condition simulated. Additional consideration can be given to the parameters used in the model to make closer

connections with experimental measurements. The effects of the different parameters in controlling the oxygen absorption can also be studied with this model.

In order to simulate different tidal volumes using the exchange model proposed in this thesis, more needs to be known regarding how the oxygen transport properties of the tissue are affected by changing the expansion of the alveoli. For larger tidal volumes, more oxygen will be drawn into the lungs and a larger surface area will be available for exchange. When the alveoli expand, the thickness of the blood gas barrier must decrease so conserve the volume of the pulmonary cells. Any resulting changes in the oxygen transport properties would change the method used to calculate the exchange coefficient described in Section 5.1.3. Although the approach described in this work would accommodate the increase in the amount of oxygen available with the increased tidal volume, any change in the transport properties of the tissue would not be included. Therefore, before this model can be used to simulate additional tidal volumes, more needs to be known regarding the effects of tidal expansion on the oxygen transport properties of the tissue.

Presently, the tissue is simulated using a large oxygen diffusivity value, making it possible for the tissue to absorb oxygen without increasing its the oxygen concentration during respiration. Allowing the oxygen concentration of the tissue to change would make it possible to simulate deoxygenated blood entering the alveolar tissue while oxygenated blood leaves the tissue. However the method for simulating the exiting blood needs to be determined.

The crude approximation used to determine the amount of carbon dioxide exhaled can be replaced by another volume-averaged species transport equation. The oxygen transport equation closed in Chapter 5 can be used for carbon dioxide exchange although carbon dioxide specific parameters must be applied. This will make it necessary to include a changing air density to accommodate the changing concentration of two gases with the inclusion of the nitrogen. This addition would better approximate the amount of carbon dioxide exchanged per breath than the system currently implemented in the model.

This model provides a framework for calculating species exchange within the alveolar region of the lung. The volume-averaged approach to the oxygen transfer equation described in this thesis can be implemented in the lung model developed by DeGroot [27], removing many of the assumptions made to simulate oxygen exchange with a through flow by including mesh motion. With both models integrated, it will be possible to determine both oxygen and carbon dioxide concentration throughout a working model of the human lungs.

A complete model of exchanging, expanding working lungs could be used to study the affects of lung diseases by changing the parameters of the tissue. The affects of these changes on the amount of oxygen absorbed by the lungs could be examined without the need for clinical trials. Additionally, this model could be used study the absorption of other inhaled substances such as medications or toxins. Additional volume-averaged species transport equations can be introduced which could calculate the dispersion of these substances throughout the lungs.

REFERENCES

[1] Bates, J. H. T.. 2009, *Lung Mechanics: An Inverse Modeling Approach*, Cambridge University Press, New York.

[2] Waite, L., and Fine, J., 2007, *Applied Biofluid Mechanics*, The McGraw-Hill Companies, Inc, New York.

[3] Keener, J., and Sneyd, J., 2009, *Mathematical Physiology II: Systems Physiology*, Springer Science + Business Media, New York.

[4] Waugh, A., and Grant, A., 2001, *Ross and Wilson Anatomy and Physiology in Health and Illness, Ninth Edition,* Churchill Livingstone, London.

[5] Russell, P.J., Wolfe, S.L., Hertz, P.E., Starr, C., and McMillan, B., 2008, *Biology Volume 3: The Dynamic Science, Volume 3*, Thompson Books/Cole, Canada.

[6] Fung, Y.C., 1997, *Biomechanics Circulation, Second Edition*, Springer-Verlag, New York.

[7] Schilder, D. P., Roberts, A., and Fry, D. L., 1963, "Effects of Gas Density and Viscosity on the Maximal Expiratory Flow-volume Relationship," J. Clinical Investigation, **42**, 1705-1713.

[8] Betchen, L., Straatman, A. G., and Thompson, B.E., 2006, "A Nonequilibrium Finite-volume Model for Conjugate Fluid/Porous/Solid Domains.," Numerical Heat Trans. Part A., **49**, 543-565.

[9] West, J. B., 2008, *Repiratory Physiology: The Essentials, Eighth Edition*, Lippincott Williams & Wilkins, Baltimore.

[10] Roughton, F. J. W., and Forster, R. E., 1957, "Relative Importance of Diffusion and Chemical Reaction Rates in Determining Rate of Exchange of Gases in the Human Lung, with Special Reference to True Diffusing Capacity of Pulmonary Membrane and Volume of Blood in the Lung Capillaries," J. Appl. Phys., **11**, 290-301.

[11] Tschanz, S. A., Makanya, A. N., Haenni, B., and Burri, P. H., 2003, "Effects of Neonatal High-dose Short-term Glucocorticoid Treatment on the Lung: A Morphologic and Morphometric Study in the Rat," Pediatric Research, **53**, 72-80.

[12] Kleinstreuer, C., 2006, *Biofluid Dynamics Principles and Selected Applications*, CRC Press, Boca Raton.

[13] Lin, C-L., Tawhai, M.H., McLennan, G., & Hoffman, E.A., 2009, "Multiscale Simulation of Gas Flow in Subject-specific Models of the Human Lung," IEEE Engineering in Medicine & Biology Magazine, **28**, 25-33.

[14] Nakayama, A., Kuwahara, F., and Sano, Y., 2009, "Why do we have a bronchial tree with 23 levels of bifurcation?" Heat & Mass Trans., **45**, 351-354.

[15] Tian, G., and Worth Longest, P., 2010, "Development of a CFD Boundary Condition to Model Transient Vapor Absorption in the Respiratory Airways," J. Biomed. Eng., **132**, 051003-1-13.

[16] Radhakrishnan, H., and Kassinos, S., 2009, "CFD Modeling of Turbulent Flow and Particle Deposition in Human Lungs," 31st Annual Int. Conf. of IEEE EMBS.

[17] Gemci, T., Ponyavin, V., Chen, Y., Chen, H., and Collins, R., 2008, "Computational Model of Airflow in Upper 17 Generations of the Human Respiratory Tract," J. Biomech., **41**, 2047-2054.

[18] Weibel, E.R., 1963, *Morphometry of the human lung*, Springer-Verlag, New York.

[19] Harding, E. M., and Robinson R. J., 2010, "Flow in a Terminal Alveolar Sac Model with Expanding Walls using Computational Fluid Dynamics," Inhal. Toxicol., **22**, 669-678.

[20] Kumar, H., Tawhai, M. H., Hoffman, E., A., and Lin, C.-L., 2009, "The Effects of Geometry on Airflow in the Acinar Region of the Human Lung," J. Biomech., **42**, 1635-1642.

[21] Oakes, J. M., Day, S., Weinstein, S. J., and Robinson, R. J., 2010, "Flow Field Analysis in Expanding Healthy and Emphysematous Alveolar Models using Particle Image Velocimetry," J. Biomed. Eng., **132**, 021008-1-9.

[22] Tsuda, A., Filipovic, N., Haberthuer, D., Dickie, R., Matsui, Y., Stampanoni, M., and Schittny, J.C., 2008, "Finite Element 3D Reconstruction of the Pulmonary Acinus Imaged by Synchrotron X-ray Tomography," J. Appl. Physiol., **105**, 964-976.

[23] Yang, N., and Vafai, K., 2006, "Modeling of Low-density Lipoprotein (LDL) Transport in the Artery – Effects of Hypertension," Int. J. Heat & Mass Trans., **49**, 850-867.

[24] Yang, N., and Vafai, K., 2008, "Low Density Lipoprotein (LDL) Transport in an Artery – A Simplified Analytical Solution," Int. J. Heat & Mass Trans., **51**, 497-505.

[25] Koulich, V., Lage, J. L., Hsia, C. C. W., and Johnson, R. L., Jr., 1999, "A Porous Medium Model of Alveolar Gas Diffusion," J. Porous Media, **2**, 263-275.

[26] Kuwahara, F., Sano, Y., Lui, J., and Nakayama, A., 2009, "A Porous Media Approach for Bifurcating Flow and Mass Transfer in the Human Lung," J. Heat Trans., **131**, 101013-1-5.

[27] DeGroot, C.T., 2012, "Numerical Modelling of Transport in Complex Porous Media: Metal Foams to the Human Lung," Ph.D. thesis, Mechanical and Materials Engineering, The University of Western Ontario.

[28] Whitaker, S., 1997, *Fluid Transport in Porous Media Chapter 1*. Bath: Computational Mechanics Publications.

[29] DeGroot, C.T., 2009, "Numerical Modelling of Thermal Dispersion and Viscous Effects in High – Conductivity Porous Materials," M.E.Sc. thesis, Mechanical and Materials Engineering, The University of Western Ontario.

[30] Rhie, C.M., and Chow, W.L., 1983, "Numerical Study of Turbulent Flow Past an Airfoil with Trailing Edge Separation," AIAA J., **21**, 1525-1532.

[31] Weibel, E. R., Sapoval, B., and Filoche, M., 2005, "Design of Peripheral Airways for Efficient Gas Exchange," Respiratory Physiology & Neurobiology, **148**, 3-21.

[32] Ochs, M., Nyengaard, J.R., Jung, A., Knudsen, L., Voigt, M., Wahlers, T., Richter, J., and Gundersen, H.J.G., 2004, "The Number of Alveoli in the Human Lung," Am. J. Respir. Crit. Care Med., **169**, 120-124.

[33] Incropera, F.P., Dewitt, D.P., Bergman, T.L., and Lavine, A.S., 2007, *Fundamentals of Heat and Mass Transfer, Sixth Edition*, John Wiley and Sons, Hoboken, NJ.

[34] Ellis, C.G., course notes from *MBP 3507G Analysis of Oxygen Transport in Biological Systems*, Department of Medical Biophysics, The University of Western Ontario.

[35] Sasaki, N., Horinouchi, H., Ushiyama, A., and Minamitani, H., 2012, "A New Method for Measuring the Oxygen Diffusion Constant and Oxygen Consumption Rate of Arteriolar Walls," Keio J. Med., **61 (2)**: 57-65.

APPENDIX A

ADDITIONAL CODE VERIFICATION AND RESULTS

A.1 POROUS PLUG FLOW RESULTS

To validate the velocity and pressure coupling, a porous plug flow test was completed. The case was run with a Darcy number of 10^{-3}, $Re_H = 1$ and $\varepsilon = 0.7$ for a channel of length $8H$, height H. The channel was divided into three sections, the first and last fluid regions were of length $3H$ while the porous plug in the centre had length $2H$. In accordance with Betchen et al [8], each section contained 20 control volumes in the x-direction, 21 control volume in the y-direction and three control volumes in the z-direction. The mesh was refined along the interfaces to give better results. The boundary conditions for the velocity were fully developed flow at the inlet, Eq. A.1, and zero derivative conditions in all three directional components at the outlet,

$$u(0, y) = \frac{6Uy}{H}\left(1 - \frac{y}{H}\right) \tag{A.1}$$

where u is the velocity across the inlet, U is the maximum velocity, and y is the height across the inlet.

The pressure at the outlet was set to zero using a Dirichlet boundary condition and extracted at all other surfaces using a Neumann boundary condition. Using an upwind differencing convection scheme the results for both pressure and velocity can be seen in Figures A.1 and A.2 respectively. These results closely match those of Betchen et al [8]. However, both figures show a slight wiggle at the interface between the fluid and porous regions. The interface conditions were preexisting in the code and were not dealt with in this work. The domain used for the lung model was porous only, containing no interfaces; therefore any wiggle at the interface was not a concern in this work.

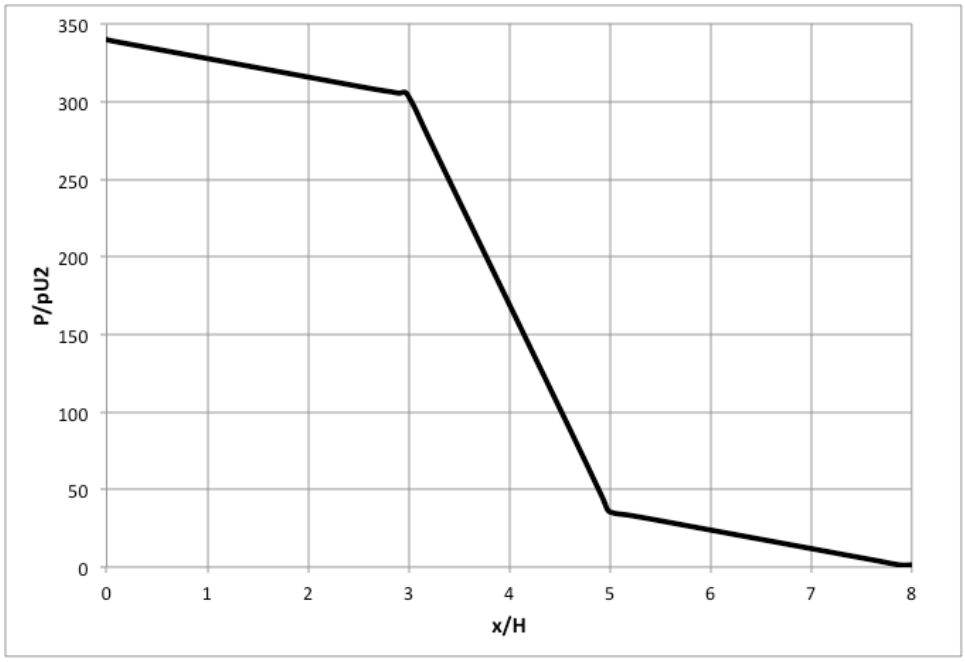

Figure A.1. *The pressure across the modelled domain, the location of the porous plug is clearly visible.*

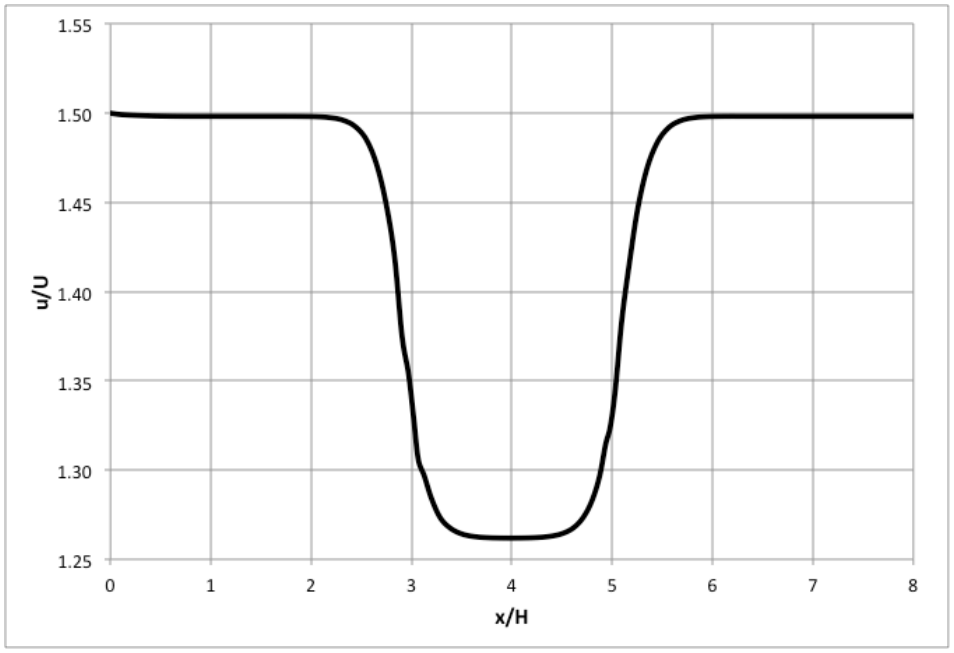

Figure A.2. *The velocity profile, showing a clear reduction in velocity across the porous plug.*

A.2 TERMINAL TUBE RESULTS

The amount of oxygen absorbed per breath has been plotted in Figures A.3, A.4 and A.5 for cases one, two and three as described in Table 4.1 respectfully.

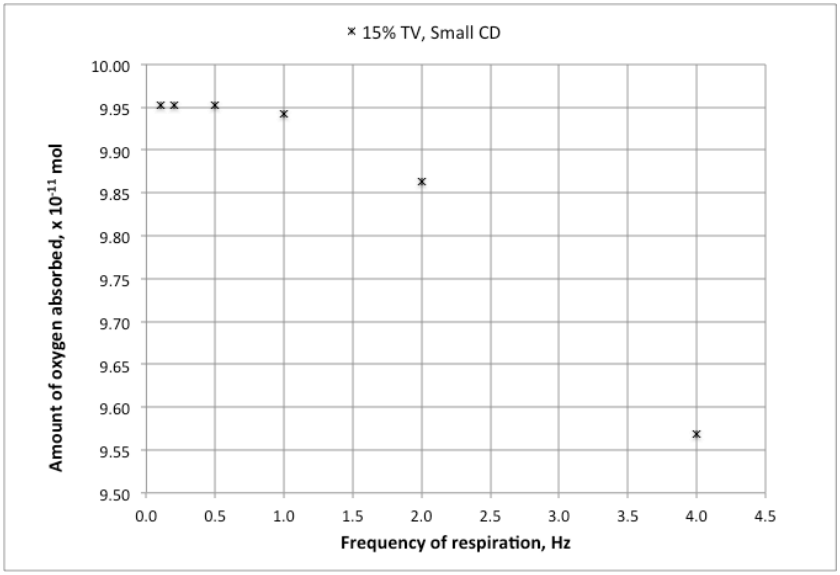

Figure A.3. *Case 1: The amount of oxygen absorbed per breath for the 15% tidal volume case with respect to frequency of respiration. TV = tidal volume, CD = concentration difference between the inlet and the wall.*

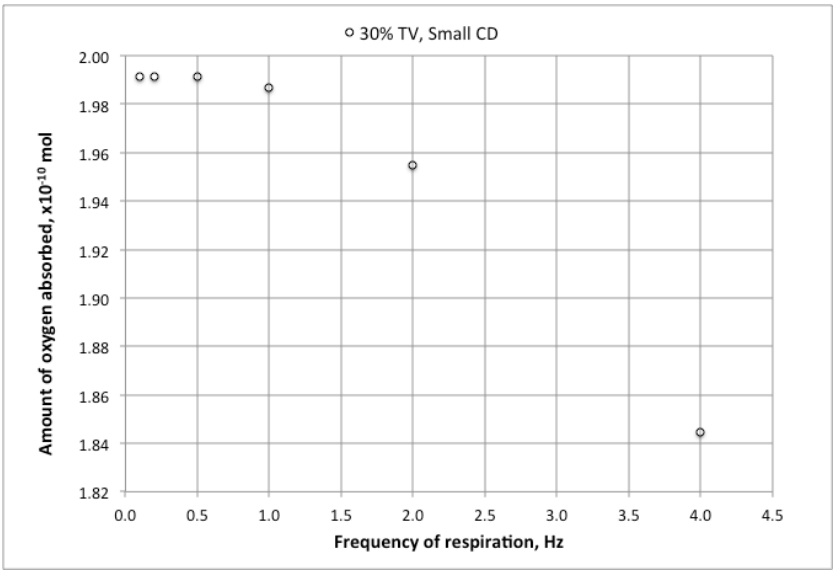

Figure A.4. *Case 2: The amount of oxygen absorbed per breath for the 30% tidal volume case with respect to the frequency of respiration. TV = tidal volume, CD = concentration difference between the inlet and the wall.*

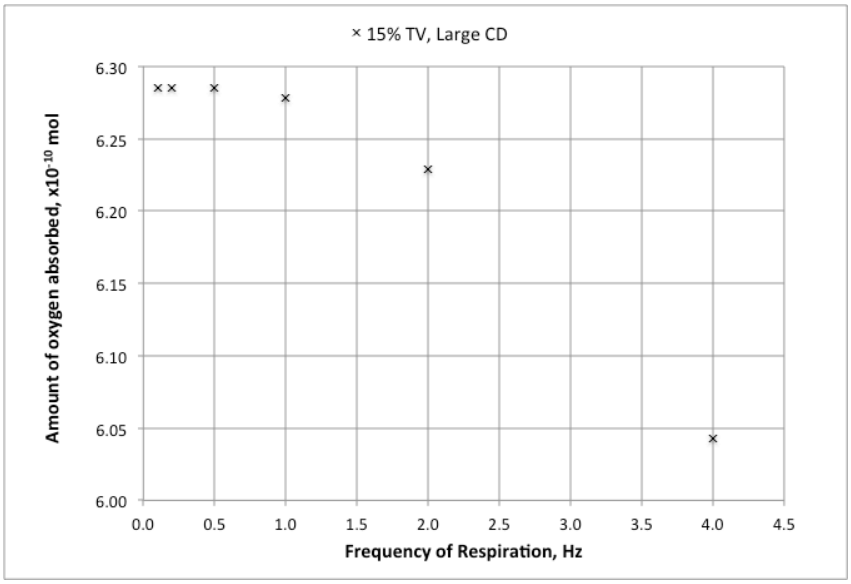

Figure A.5. *Case 3: The amount of oxygen absorbed per breath for the 15% tidal volume case with respect to the frequency of respiration. The concentration difference between the inlet and alveolar wall for this case was for inhaled air with 50% oxygen. TV = tidal volume, CD = concentration difference between the inlet and the wall.*

VITA

Name:	Chelsea E. Johnson
Post-secondary Education and Degrees:	The University of Western Ontario London, Ontario, Canada 2011–2013 M.E.Sc.
	The University of Western Ontario London, Ontario, Canada 2006-2011 B.E.Sc.
	The University of Western Ontario London, Ontario, Canada 2006-2011 B.Sc.
Honours and Awards:	Natural Sciences and Engineering Research Council (NSERC) Alexander Graham Bell Canada Graduate Scholarship (Masters) May 2012 – April 2013
	Ontario Graduate Scholarship (OGS) May 2011 – April 2012
Related Work Experience:	Teaching Assistant Department of Mechanical and Materials Engineering The University of Western Ontario 2011–2013